

EFFECT OF ECAP AND SUBSEQUENT HEAT TREATMENTS
ON MICROSTRUCTURE AND MECHANICAL PROPERTIES
OF 2024 ALUMINUM ALLOY

A THESIS SUBMITTED TO
THE GRADUATE SCHOOL OF NATURAL AND APPLIED SCIENCES
OF
MIDDLE EAST TECHNICAL UNIVERSITY

BY

EBRU SARALOĞLU

IN PARTIAL FULFILLMENT OF THE REQUIREMENTS
FOR
THE DEGREE OF MASTER OF SCIENCE
IN
METALLURGICAL & MATERIALS ENGINEERING

AUGUST 2008

Approval of the thesis:

**EFFECT OF ECAP AND SUBSEQUENT HEAT TREATMENTS
ON MICROSTRUCTURE AND MECHANICAL PROPERTIES
OF 2024 ALUMINUM ALLOYS**

submitted by **EBRU SARALOĞLU** in partial fulfillment of the requirements for the degree of **Master of Science in Metallurgical and Materials Engineering, Middle East Technical University** by,

Prof. Dr. Canan Özgen
Dean, Graduate School of **Natural and Applied Sciences** _____

Prof. Dr. Tayfur Öztürk
Head of Department, **Metallurgical and Materials Eng.** _____

Prof. Dr. C. Hakan Gür
Supervisor, **Metallurgical and Materials Eng. Dept., METU** _____

Prof. Dr. Tayfur Öztürk
Co-Supervisor, **Metallurgical and Materials Eng. Dept., METU** _____

Examining Committee Members

Prof. Dr. Cevdet Kaynak
Metallurgical and Materials Eng. Dept., METU _____

Prof. Dr. C. Hakan Gür
Metallurgical and Materials Eng. Dept., METU _____

Prof. Dr. Tayfur Öztürk
Metallurgical and Materials Eng. Dept., METU _____

Assist. Prof. Dr. Caner Durucan
Metallurgical and Materials Eng. Dept., METU _____

Assist. Prof. Dr. Besim Baranoğlu
Production Eng. Dept., Atılım University _____

Date: 22 / 08 / 2008

I hereby declare that all information in this document has been obtained and presented in accordance with academic rules and ethical conduct. I also declare that, as required by these rules and conduct, I have fully cited and referenced all material and results that are not original to this work.

Name, Last name: Ebru Saralođlu

Signature:

ABSTRACT

EFFECT OF ECAP AND SUBSEQUENT HEAT TREATMENTS ON MICROSTRUCTURE AND MECHANICAL PROPERTIES OF 2024 ALUMINUM ALLOY

Saralođlu, Ebru

M.Sc., Department of Metallurgical and Materials Engineering

Supervisor : Prof. Dr. C. Hakan Gr

Co-supervisor: Prof. Dr. Tayfur ztrk

August 2008, 85 pages

Severe plastic deformation (SPD) results in ultra-fine grain sizes in metals and alloys. Equal channel angular pressing (ECAP) is one of the special SPD methods aiming to introduce high plastic strains into the bulk materials without changing their cross section. ECAP results in improvement in hardness and strength while still satisfying acceptable ductility level. The combined effects of ECAP and subsequent heat treatments, i.e. post-aging and post-annealing, on the microstructure and hardness of the 2024 aluminum alloy were investigated. An ECAP die with 120° channel angle was constructed. Subgrain formation, increase in dislocation density and dislocation tangling were observed after ECAP, and subgrain growth was detected after post annealing. The specimens revealed higher hardness values after ECAP at room temperature, and further increase in hardness was observed following post-aging at 80°C, 100°C and 190°C. Effect of the aging temperature on the deformed specimens was investigated, and the aging behaviors of the severely deformed and undeformed samples at 190°C were compared.

Keywords: 2024 Al-alloy, ECAP, Aging, Microstructure, Hardness

ÖZ

EKAP VE SONRASINDA UYGULANAN YAŞLANDIRMA VE TAVLAMA İŞLEMLERİNİN 2024 ALÜMİNYUM ALAŞIMININ İÇYAPI VE MEKANİK ÖZELLİKLERİNE ETKİSİ

Saralođlu, Ebru

Yüksek Lisans, Metalurji ve Malzeme Mühendisliđi Bölümü

Tez Yöneticisi : Prof. Dr. C. Hakan Gür

Ortak Tez Yöneticisi: Prof. Dr. Tayfur Öztürk

Ađustos 2008, 85 sayfa

Aşırı plastik deformasyon ile metallerde ve alaşımlarda aşırı ince tane boyutlarına ulaşılabilir. Eş kanallı açısız presleme (EKAP) hacimli malzemelere kesitlerini deđiştirmeden yüksek plastik gerinimler yüklemeyi amaçlayan aşırı plastik deformasyon yöntemlerinden biridir. EKAP, kabul edilebilir süneklik düzeyini sağlarken, sertlik ve mukavemette artışa sebep olmaktadır. EKAP ve takiben ısı işlemlerin (yaşlandırma ve tavlama) 2024 alüminyum alaşımlarının mikro yapı ve sertliklerine etkileri araştırılmıştır. 120° kanal açılı bir EKAP kalıbı yapılmıştır. EKAP sonrasında; tanecik oluşumu, dislokasyon yoğunluğunda artış ve dislokasyon dolanımı gözlenmiştir; takip eden tavlama işlemiyle tanecik büyümesi tespit edilmiştir. Oda sıcaklığında yapılan EKAP işleminden sonra numunelerin sertliđi artmıştır. EKAP işlemini takiben uygulanan 80°C, 100°C, 190°C sıcaklıklarda yaşlandırma işlemiyle sertlikte ilave artış sağlanmıştır. Deforme edilmiş numunelerde yaşlandırma sıcaklığının etkisi araştırılmış ve aşırı deforme edilmiş ve edilmemiş numunelerin 190°C'deki yaşlandırma davranışları karşılaştırılmıştır.

Anahtar Kelimeler: 2024 alüminyum alaşımı, EKAP, Yaşlandırma, Mikroyapı, Sertlik

To My Family;

Attila Saralođlu

Hatice Saralođlu

Kaan Saralođlu

ACKNOWLEDGEMENTS

I wish to express my deepest gratitude to my supervisor Prof. Dr. C. Hakan Gür and co-supervisor Prof. Tayfur Öztürk for their guidance, criticism and support throughout the thesis.

My special thanks go to Ziya Esen for his encouragements and helps. I have also benefited by advice and guidance from him.

I would also like to thank Özgür Duygulu for his crucial contribution which made him a backbone of this research in the final stages.

Many thanks go to Ünal Pehlivan for using his times during the experiments carried out in Ostim.

I am grateful to Caner Şimşir for sharing his precious ideas and advice.

Furthermore, I would like to thank my colleagues Betül Pelin Maradit, Burcu Kayıplar and others for their moral support and friendship.

Thanks go to Evren Tan for his help at the beginning of the research.

Finally, I thank my dad, mother and brother; Attila Saraloğlu, Hatice Saraloğlu and Kaan Saraloğlu respectively for supporting me throughout all my life.

This study was supported by the TUBITAK project 105M174.

TABLE OF CONTENTS

ABSTRACT	iv
ÖZ	v
ACKNOWLEDGEMENTS	vii
TABLE OF CONTENTS	viii
CHAPTER	
1. INTRODUCTION	1
2. THEORY AND LITERATURE SURVEY	3
2.1 2024 Aluminum Alloy and Strengthening Mechanisms	3
2.1.1 Main Properties and Application	3
2.1.2 Strengthening by Strain Hardening and Grain size reduction	5
2.1.3 Strengthening from fine particles	6
2.1.3.1 Precipitation (Age) Hardening	6
2.1.3.2 Dispersion Hardening	7
2.2 Severe Plastic Deformation (SPD)	9
2.3 Equal Channel Angular Pressing (ECAP)	10
2.3.1 Parameters affecting ECAP Process	12
2.3.2 Advantages of ECAP over Conventional Deformation Methods	14
2.3.3 Microstructural and Mechanical Improvement by ECAP	17
2.4 Heat Treatment after ECAP	22
2.4.1 Age Hardening	22
2.4.2 Annealing	32
3. EXPERIMENTAL PROCEDURE	36
3.1 Material	36
3.2 Die Design	37
3.2.1 Initial Trials	37

3.2.2 Optimization Studies	45
3.2.3 Final Decision	48
3.3 Experimental Set-up	50
3.4 Heat Treatment	50
3.5 Characterization of Samples	53
3.5.1 X-Ray Diffraction (XRD).....	53
3.5.2 Microstructure	53
3.5.3 Hardness Measurements	54
4. RESULTS AND DISCUSSION	55
4.1 Results of X-ray Measurements	55
4.2 Microstructural Investigations	57
4.2.1 Observations via Optical Microscopy and Scanning Electron Microscopy	57
4.2.2 Observations via Transmission Electron Microscopy	59
4.3 Results of Hardness Measurements	69
5. CONCLUSION	71
REFERENCES.....	72
APPENDICES	
A. EDS ANALYSIS	82
B. X-RAY MAP ANALYSIS	85

LIST OF TABLES

TABLES

Table 2.1 Rotation angles and directions for possible routes [51].....	11
Table 2.2 TEM micrographs of 7050 Al-alloy for 4 different conditions [74].....	24
Table 3.1 Comparison of the spectral analysis of the alloy used and standard 2024 Al-alloy.....	35
Table 3.2 Hardness values of the 6066 Al-alloy samples.....	37
Table 3.3 Hardness values of the 5083 Al-alloy specimens	41
Table 3.4 ECAP trials of 2024 Al-alloy specimens using the double channel die	44
Table 3.5 ECAP trials of 2024 Al-alloy specimens using the single channel die	46
Table 3.6 Aging temperatures and durations.....	49
Table 3.7 Loads used in Heckert analogue hardness machine.....	51
Table 4.1 Chemical compositions of the matrix and inclusion of the solutionized 2024 Al-(EDS analysis).....	55
Table 4.2 Chemical composition of T-phase dispersoid by EDS analysis	57
Table 4.3 Chemical composition of the precipitates in aged 2024 Al-alloy (EDS analysis).....	64
Table 4.4 Hardness values of 2024 Al alloy specimen in different conditions	66

LIST OF FIGURES

FIGURES

Figure 2.1 Portion of aluminum-copper binary phase diagram showing the temperature ranges for annealing, precipitation heat treating, and solution heat treatment [1].....	3
Figure 2.2 Microstructure of 2024-T3 sheet 500X [1]	3
Figure 2.3 TEM micrograph of 2024 Al-alloy showing precipitates S'' and S' a. 190 °C/12h, b. 250 °C/10min [10].....	7
Figure 2.4 Rod-like T-phase dispersoids (Al ₂₀ Cu ₂ Mn ₃) in the 2024 Al-alloy solutionized at 493 °C for 10h [11]	7
Figure 2.5 Principal illustration of the ECAP process [4, 49]	9
Figure 2.6 Four fundamental processing routes [50]	10
Figure 2.7 Schematic illustration of the ECAP die showing the channel angle Φ and the arc angle Ψ [12]	12
Figure 2.8 ECAP die with controlled backpressure [62]	13
Figure 2.9 Comparison of yield strength and ductility of ECAPed and cold-rolled 3004 Al-alloy [66]	15
Figure 2.10 Variation of grain size with annealing temperature for various Al-alloys [65]	16
Figure 2.11 TEM micrograph of ECAPed 6061 Al-alloy [60]	17
Figure 2.12 TEM micrographs and corresponding SAED patterns of a. unECAPed b. one- pass ECAPed single phase Al-1.7 at% Cu alloy [71]	18
Figure 2.13 Dislocation tangling after cyro-rolling of 2024 Al-alloy at a strain of a. ~15% b. ~40% c. ~80% [11]	19
Figure 2.14 Variation of grain size with annealing temperature for various Al-alloys [65]	20

Figure 2.15 The stress–strain curves of the unECAPed and ECAP processed 2024 Al alloys [70].....	20
Figure 2.16 a. 0.2% proof stress b. elongation to failure versus equivalent strain graphs of various Al-alloys after ECAP [65].....	21
Figure 2.17 TEM micrographs and corresponding SAED patterns of 2024 Al-alloy a. PA specimen after two passes b. PA specimen after eight passes c. OA specimen after two passes and d. OA specimen after eight passes [38]	23
Figure 2.18 TEM micrograph and corresponding SAED patterns of 6061 Al-alloy a. FC-ECAPed and b. WQ-ECAPed 6061 Al-alloy [75].....	25
Figure 2.19 Age hardening profiles of a. unECAPed and b. ECAPed 2024 Al-alloy specimens aged at 100 °C and 175 °C [70].....	26
Figure 2.20 Age hardening profiles of ECAPed and unECAPed 6061 Al-alloy specimens a. at 175 °C b. at 100 °C [72].....	26
Figure 2.21 Stress-strain curves of only peak aged (175 °C, 8h), 4-pass ECAPed+peak aged (100 °C, 48h) and only ECAPed 6061 Al-alloy specimens [72] .	27
Figure 2.22 a. Effect of aging temperature on strength and ductility in 6-pass ECAPed AlMgSi alloy b. Age hardening profiles of ECAPed and unECAPed alloys at 110 and 175 °C [64]	28
Figure 2.23 TEM micrograph of four pass ECAPed and aged (100 °C / 48h) 6061 Al-alloy [72].....	29
Figure 2.24 Bright field TEM images and corresponding SAED patterns of a. aged (100 °C, 24h) b. one pass ECAPed+aged (100 °C / 24h) c. eight pass ECAP+aged (100 °C / 24h) d. Dark-field image of eight pass ECAP+aged (100 °C / 24h) of Al-1.7at% Cu alloy [71].....	30
Figure 2.25 TEM micrographs of the ECAPed + aged (100 °C / 20h) 2024 Al-alloy a. Low magnification, b. high magnification [70].....	31
Figure 2.26 Schematic view of grain and subgrain (cell) structure in aluminum [77] ..	32
Figure 3.1 General experimental layout.....	34
Figure 3.2 Vertical axis hydraulic press with 30 ton capacity	36

Figure 3.3 ECAP die with 90° channel angle	36
Figure 3.4 Two side views of (a) unECAPed (b) ECAPed without prior heat treatment (c) annealed at 450°C for 60h and ECAPed (d) annealed at 450°C for 120h and ECAPed specimens.	37
Figure 3.5 Variation of hardness in 6066 Al-alloy samples as a function of annealing time at 450 °C	38
Figure 3.6 Coding of specimen surfaces	39
Figure 3.7 Hardness profile along the cross-section of 6066 Al-alloy after ECAP	39
Figure 3.8 Variation of hardness in 5083 Al-alloy samples as a function of the annealing time at 415 °C	40
Figure 3.9 Photographs of 5083 Al-alloy specimens in (a) unECAPed (b) ECAPed (c) Annealed (415°C / 144h) + ECAPed conditions	41
Figure 3.10 Change in square patterns in 5083 Al alloy specimens after ECAP.	42
Figure 3.11 Pattern change in the lateral section of 5083 Al alloy specimen after ECAP	42
Figure 3.12 Pattern change in the lateral section of 6066 Al alloy specimen after ECAP	42
Figure 3.13 ECAP die with double 120° channel angle having cross-section with 18mm diameter	43
Figure 3.14 Horizontal axis hydraulic press.	48
Figure 3.15 (a) ECAP die with 120 ° channel angle having circular (18 mm Φ) cross-section and (b) the punch of the die.	48
Figure 3.16 Schematic view of the oil bath	49
Figure 4.1 X-ray diffraction peaks of (111) plane for specimens in different conditions.	53
Figure 4.2 X-ray diffraction peaks of (111) plane for annealed and ECAPed specimens.	53

Figure 4.3 Microstructure of 2024 Al-alloy in the solutionized condition (a) Optical micrograph (100X), (b) Grain size distribution.	55
Figure 4.4 SEM micrographs of the solutionized 2024 Al-alloy.	56
Figure 4.5 a. TEM micrograph of 2024 Al-alloy specimen in as-received condition b. Rodlike shaped dispersoid.	56
Figure 4.6 TEM micrographs of 2024 Al-alloy in the solutionized condition.	58
Figure 4.7 TEM images of ECAPed 2024 Al-alloy a. Bright field b. dark field TEM image c. SAED patterns.	59
Figure 4.8 TEM micrographs showing dislocation structure of ECAPed 2024 Al-alloy	61
Figure 4.9 a. TEM micrographs and b. grain size distribution of post-ECAP annealed specimen.	62
Figure 4.10 a. Dark field image b. Bright field image of the unECAPed and aged (190°C / 12h) specimen 1.	63
Figure 4.11 a. Dark field image b. Bright field image of the unECAPed and aged (190°C / 12h) specimen 2.	63
Figure 4.12 TEM micrograph of the ECAPed and age hardened (190 °C / 2h) specimen.	65
Figure 4.13 TEM micrograph of the aged (190°C / 12h) specimen	65
Figure 4.14 Hardness versus aging time (in seconds) graph of ECAPed and unECAPed specimens	67

CHAPTER 1

INTRODUCTION

Lightweight structural materials like aluminum alloys have attracted great interest due to their high strength to weight ratio. So, improving mechanical properties as well as formability of these alloys becomes an important issue. The demand for ultra fine grain sized (UFG) materials, having grain sizes in the submicrometer range, produced via severe plastic deformation have increased in recent years in order to improve mechanical properties. Equal channel angular pressing (ECAP) which is one of the severe plastic deformation methods, imposes high strains on relatively large samples to obtain ultrafine grain sizes by pressing through a specially designed die having equally sized two channels connected at a finite angle. Considerable improvements are observed especially in age hardenable Al-alloys via ECAP due to the combination effect of ECAP process and age hardening treatment since ductility retains or increases besides further increase in the mechanical properties during aging. Investigation of the effects of microstructure showed that both the increased dislocation density after ECAP and the distributed precipitates after subsequent aging contribute to the strengthening. The main parameters are aging temperature and time at this juncture.

In the present study, the effect of ECAP and subsequent aging on the Brinell hardness and the microstructure of 2024 Al-alloy via transmission electron microscopy (TEM) were investigated and the difference between age hardening profiles of ECAPed and post-ECAP aged specimens was presented. The subgrain sizes of the ECAPed and post-ECAP annealed specimens were determined via TEM micrographs and X-ray analysis results. Precipitates were observed as a result of age hardening treatment both before and after ECAP process.

In the following chapter, theory and literature review were written in order to provide an overview about the topic. Next, in the subsequent chapter, experimental procedure was constituted to explain the method and the route followed during the study. In the results and discussion chapter, micrographs were presented, hardness results were tabulated and aging graphs were drawn and finally X-ray results were shown.

Moreover, results were discussed in the light of theoretical information and compared with literature and similarities between the results of X-ray analysis and transmission electron micrographs were emphasized.

CHAPTER 2

THEORY AND LITERATURE SURVEY

2.1 2024 Aluminum Alloy and Strengthening Mechanisms

2.1.1 Main Properties and Application

Aluminum alloys are classified according to composition ranges. Among these groups 2xxx, 6xxx and 7xxx series are heat treatable. 2xxx series alloys are suitable for parts and structures that necessitate high strength to weight ratios and are often used to make truck and aircraft wheels, truck suspension parts, aircraft fuselage and wing skins and structural parts. The weldability of these alloys is limited however; some alloys have superior machinability [1].

Since 2xxx series Al-alloys has nominal copper contents ranging from 2.3 to 6.3 wt%, they are hypoeutectic alloys in aluminum-copper phase diagram where a simple eutectic is formed between the aluminum solid solution and the θ (Al_2Cu) phase. A critical feature of this region of the diagram is the shape of the aluminum solvus line (Figure 2.1). At the eutectic temperature (548.2 °C), 5.65 wt% Cu will dissolve in aluminum. At lower temperatures the amount of copper that can remain in the aluminum solid solution under equilibrium conditions drastically decreases, reaching less than 1 % at room temperature. This is the typical shape of the solvus line for precipitation hardening; if any of these alloys are homogenized at temperatures in or near the solid solution phase field, they can be strengthened by again at a substantially lower temperature [1].

2024 Al-alloy has a multiphase structure that contain $(\text{Mn,Fe})_3\text{SiAl}_{12}$, Mg_2Si , CuAl_2 , and Al_2CuMg , and rarely $(\text{Fe,Mn})\text{Al}_3$ or $(\text{Mn,Fe})\text{Al}_6$. The application of heat treatment dissolves much of the copper and magnesium but leaves some Al_2CuMg and perhaps CuAl_2 out of solution. In addition, manganese is precipitated from solid solution as $\text{Cu}_2\text{Mn}_3\text{Al}_{20}$ dispersoid. The wrought 2024-T4 product shows rounded Al_2CuMg as an undissolved excess phase, irregularly shaped particles of unreacted $(\text{Mn,Fe})_3\text{SiAl}_{12}$ and reaction product $\text{Al}_7\text{Cu}_2\text{Fe}$, besides fine $\text{Cu}_2\text{Mn}_3\text{Al}_{20}$ dispersoids. The latter causes grains during solution heat treatment to be moderately elongated and flattened. Figure 2.2 shows solutionized 2024-T3 showing CuMgAl_2 , $\text{Cu}_2\text{MnAl}_{20}$ and Cu_2FeAl_7 [1].

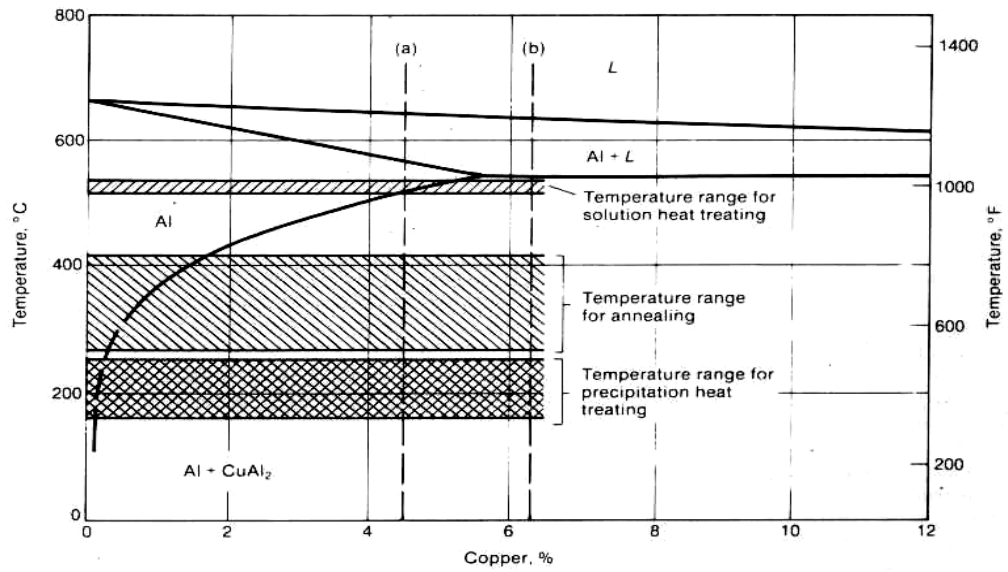


Figure 2.1 Portion of aluminum-copper binary phase diagram showing the temperature ranges for annealing, precipitation heat treating, and solution heat treatment [1].

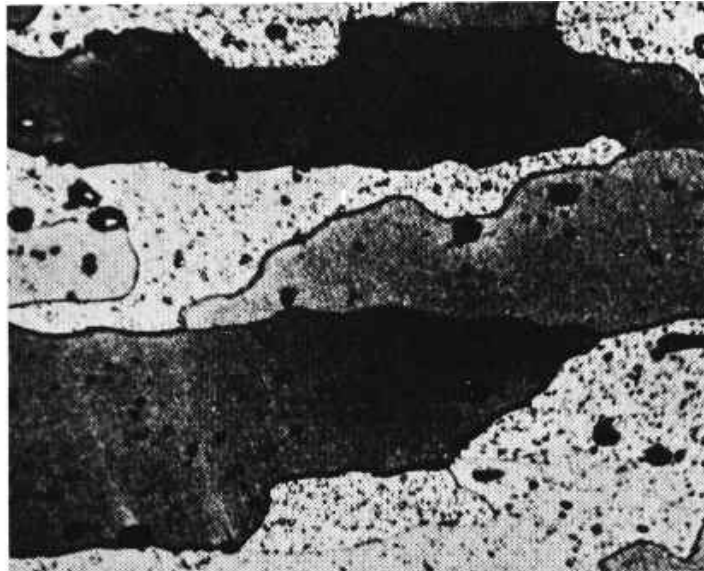


Figure 2.2 Microstructure of 2024-T3 sheet 500X [1].

2.1.2 Strengthening by Strain Hardening and Grain size reduction

Strain hardening is an important industrial process in strengthening metals through increasing hardness and strength. Dislocation density increases during plastic deformation leading to an increase in dislocation-dislocation interactions so dislocation motion is hindered. The strength can be increased by decreasing the grain size with a general relationship between yield stress and grain size [2]:

$$\sigma_0 = \sigma_i + kd^{-1/2} \quad (1)$$

σ_0 : the yield stress, σ_i : the “friction stress” representing the overall resistance of the crystal lattice to dislocation motion, k : the “locking parameter” which measures the relative hardening contribution of the grain boundaries, and d : grain diameter.

σ_i depends upon temperature much more strongly than does “ k ” and increases with strain. “ k ” is very high at very small strains when the material shows a sharp yield point. After strains greater than a few percent, “ k ” is constant for a given metal at a given temperature. Equation (1) is originated from the condition necessary for propagation of slip from grain to grain in a polycrystalline metal and hence if the number of slip systems observed in a material is small than “ k ” is found to be larger. The “ k ” values are higher in materials which show dislocation locking by impurities and smallest in pure face-centered cubic metals [3].

An equation similar to (1) describes the variation of flow stress of lamellar structures with spacing of the two component lamellae and also applies to distorted crystals containing low-angle boundaries and to subgrains; the value of “ k ” for subgrains is usually about one-half the appropriate value for the grains. A number of theoretical explanations for equation 1 have been given depending essentially on the idea of free slip in a single grain producing a pile-up of dislocations which can be viewed essentially as a type of shear crack, near the tip of which the concentrated stress depends upon the square root of the length of the crack (grain diameter) and falls off inversely as the square root of the distance from the tip of the crack. Modifications of the formulae to take account of the small length of the slipped region have been given [3].

Equation (1) can be taken as an empirical description of the effect of grain size on the strength of a polycrystalline specimen. Taking $k=2kg \text{ mm}^{-3/2}$, an increase in σ_0 of 100 kg mm^{-2} then requires a value of the grain diameter of $\sim 4000 \text{ \AA}$, at most. Such small grain sizes are not usually obtained. The increase in free energy of a metal specimen with such a grain size is less than 2 cal cm^{-3} greater than the corresponding single

crystal, so that a significant increase in strength by very marked grain refinement is possible [3].

2.1.3 Strengthening from fine particles

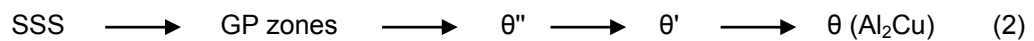
The strength of materials can be improved by the distribution of second phase particles either by dispersion hardening or precipitation hardening. Hard particles are added into the matrix in powder form and consolidation process is applied via powder metallurgy in dispersion hardening whereas strength of many alloys can be improved in solid state in precipitation hardening [2]. Second phase particles also contribute to refinement of structure and obtaining a minimal grain size during deformation [4]. In addition, in the presence of second phases, the rate of grain refinement increases in Al-alloys. This stems from the high angle grain boundary generation in the deformation zone around the particles, which then converted to submicron sized grains at low strains [5, 6]. Moreover, it was concluded that the size of the second phase particle has an effect on the rate of ultrafine grained structure formation; if the particles are coarse (~2 μ m in diameter), rapid grain refinement and the smallest grain sizes are obtained with an increased rate of HAGB formation whereas grain refinement is observed slowly when the particles are small (~10nm in diameter) [6].

2.1.3.1 Precipitation (Age) Hardening

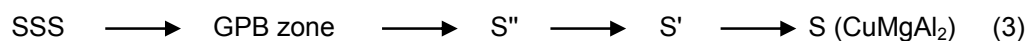
Precipitation hardening is produced by solution heat treatment at a high temperature at which the second phase is in solid solution and quenching to a low temperature at which super saturated solid solution is obtained.

Figure 2.1 shows the required solubility-temperature relationship needed in precipitation strengthening, the temperature ranges required for solution treatment and subsequent precipitate hardening in the aluminum-copper system. The equilibrium solid solubility of copper in aluminum increases as temperature increases from about 0.20% at 250 °C to a maximum of 5.65% at the eutectic melting temperature of 548 °C. For aluminum-copper alloys containing from 0.2 to 5.6% Cu, two distinct equilibrium solid states are possible. At temperatures above the lower curve (solvus), the copper is completely soluble, and when the alloy is held at such temperatures for sufficient time to permit needed diffusion, the copper will be taken completely into solid solution. At temperatures below the solvus, the equilibrium state consists of two solid

phases: solid solution, α , plus an intermetallic-compound phase, θ (Al_2Cu). When such an alloy is converted to all solid solution by holding above the solvus temperature and then the temperature is decreased to below the solvus, the solid solution becomes supersaturated and the alloy seeks the equilibrium two-phase conditions even in simple binary aluminum-copper alloys. A variety of different nonequilibrium precipitate structures is formed at temperatures below solvus. In alloys of the aluminum-copper system, a succession of precipitates is developed from a rapidly cooled supersaturated solid solution (SSS). These precipitates develop sequentially either with increasing temperature or with increasing time at temperature between room temperature and the solvus. The several stages are identified by the following notation [1]:



In Al-Cu-Mg system, precipitation sequence can be in the same sequence as given in Al-Cu system if the composition of the alloy is in $\alpha+\theta$ and $\alpha+\theta+S$ phase regions. Another sequence given in below is followed in Al-Cu-Mg alloys when Cu/Mg weight ratio is equal to 2.2 corresponding to $\alpha+S$ phase region [7]:



The presence of pre-precipitates (clusters, GBP zones) and larger phases (S'' , S' , S) at aging temperatures $\sim 200^\circ\text{C}$ is proved by high resolution electron microscopy observations in the study of Charai and his coworkers in Al-Cu-Mg alloys [8]. However, Wang and his colleagues mentioned about the presence of only GPB zone/ S'' and S precipitates after aging at 150°C [9]. In a 2024 Al-alloy, S matrix and S'' , S' (Al_2CuMg) precipitates can be shown in Figure 2.3 formed during age hardening treatment at 190°C for 12h and at 250°C for 10 min [10].

If the Al-Cu-Mg alloy with Ag addition has a composition in the $\alpha+S$ and $\alpha+\theta+S$ phase regions, the formation of Ω phase (Al_2Cu) is seen besides aforementioned precipitates [7].

2.1.3.2 Dispersion Hardening

The second phase in dispersion hardening systems has very low solubility in the matrix, even at elevated temperatures. There is no coherency between the second phase particles and the matrix whereas in precipitation hardening coherency presents

between the lattices of the precipitate and the matrix. Since the solubility of the second phase particles is very low, these alloys are resistant to recrystallization and grain growth due to dispersion of particles finely [2].

The main dispersoid in 2024 Al-alloys is $\text{Al}_2\text{Cu}_2\text{Mn}_3$ which is in rod-like shape given in Figure 2.4 [11].

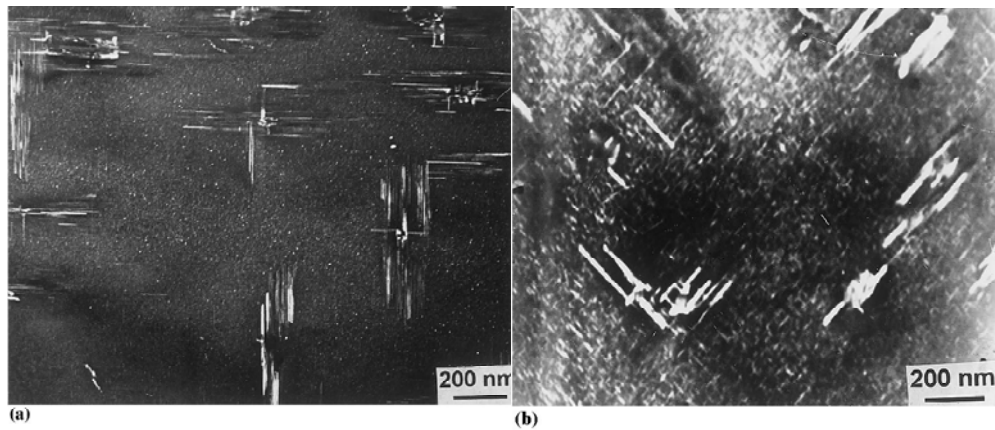


Figure 2.3 TEM micrograph of 2024 Al-alloy showing precipitates S'' and S' [10]
a. 190°C/12h, **b.** 250°C/10min.

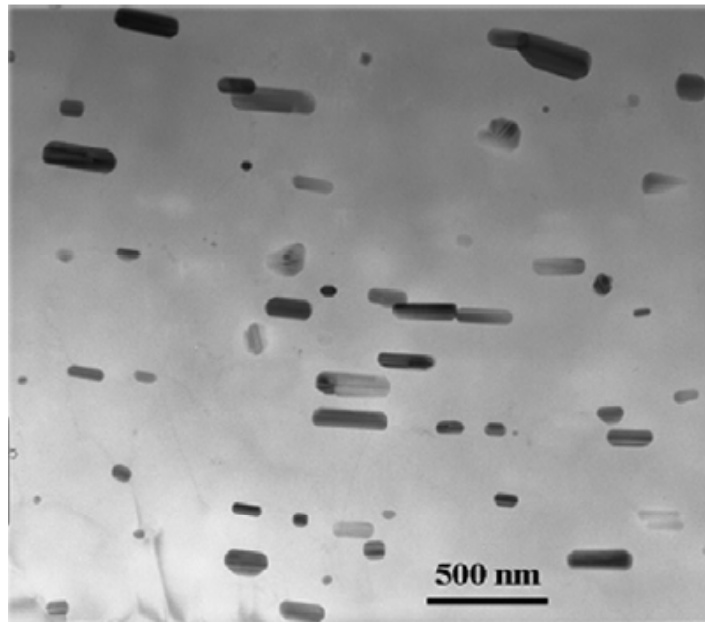


Figure 2.4 Rod-like T-phase dispersoids ($\text{Al}_{20}\text{Cu}_2\text{Mn}_3$) in the 2024 Al-alloy solutionized at 493 °C for 10h [11].

2.2 Severe Plastic Deformation (SPD)

In recent years, there is an increased interest in bulk nano-structured materials with unique properties using severe plastic deformation (SPD) methods instead of conventional deformation processes such as rolling, drawing, extrusion [4, 12]. SPD methods are preferred due to the ability of producing nanostructured materials in macroscopic volume whereas the products of traditional deformation methods are thin samples such as wires, foils [13]. Heavy deformations can be applied at low temperatures by cold rolling or drawing resulting in significant refinement of the structure with grain sizes in the range 1-10 μm . However, the resulting structures are usually substructures of a cellular type having boundaries with low angle misorientations. On the other hand, SPD processed materials contain ultra fine-grained structures of a granular type containing mainly high angle grain boundaries [4].

Twist extrusion (TE), multidirectional forging (MDF) [14, 15], high-pressure torsion (HPT) [16-23], ECA pressing [16, 17, 22, 24-42] are some of the special mechanical

methods of deformation providing large deformations at relatively low temperatures in which the initial dimensions of the samples remain the same. Among these methods HPT and ECA pressing are the most popular techniques that have been experienced further development for the formation of nanostructured and ultrafine grained (UFG) aluminum [32, 41, 43] and aluminum alloys [20, 23, 28, 30, 32, 36-38, 43] , i.e. 7075, 7050, 2024, magnesium and its alloys [28, 33, 35, 40], copper [32, 34, 42, 43], nickel [32, 43], iron [39], titanium [44] and titanium alloys [21, 45] and in some cases for austenitic [22] and low carbon steel [46, 47].

2.3 Equal Channel Angular Pressing (ECAP)

Equal channel angular pressing (ECAP) process, one of the main severe plastic deformation techniques, was originated in Soviet Union in 1970s and 1980s. But the process did not attract great attention in those years, until 1990s when the documents show the importance of ECAP in producing ultrafine grain sized materials with incomparable and original properties [12].

The aim of the ECAP process is to apply extreme amount of plastic strain to the materials without any change in the cross-sectional area of the specimens which makes the process repetitive [4]. The principle of ECAP is illustrated schematically in Figure 2.5. The process can also be carried out at elevated temperatures by placing an electric furnace. The die consists of two extrusion channels with identical cross-sections that intersect at a given angle. Very high shear strain can be obtained by multiple passes through a die without any change in the billet dimensions. Thus, the formation of ultra fine homogeneous grain structure is obtained. As a result, very strong refinement of the microstructure down to the sub micrometer level may be achieved [48]. The properties of the material strongly depend on channel feeding types in a multi-pass system. The most frequently used four fundamental processing routes in literature are given in Figure 2.6. In route A, there is no rotation of the sample between repetitive pressings. In route C, there is a rotation of 180° and in route B there is a rotation of 90° . Route B_A denotes alternate rotations of $\pm 90^\circ$ and route B_C denotes a rotation of 90° in the same direction between each pressing, respectively [50].

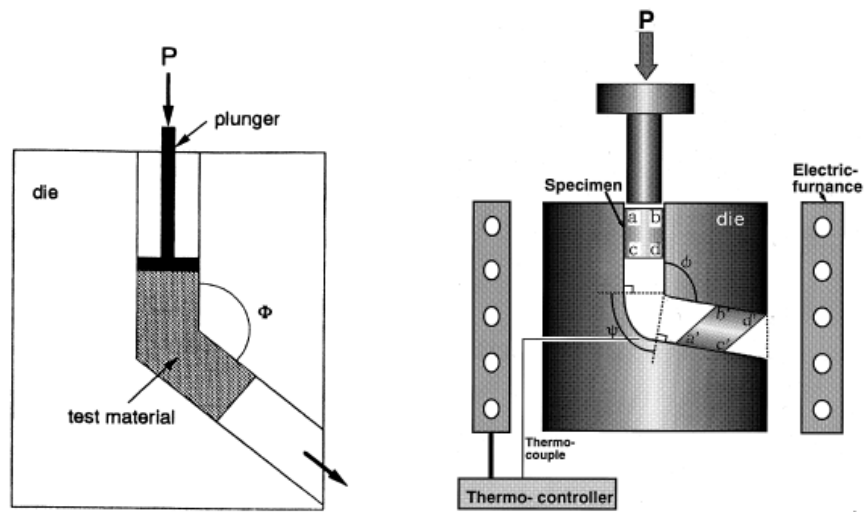


Figure 2.5 Principal illustration of the ECAP process [4, 49].

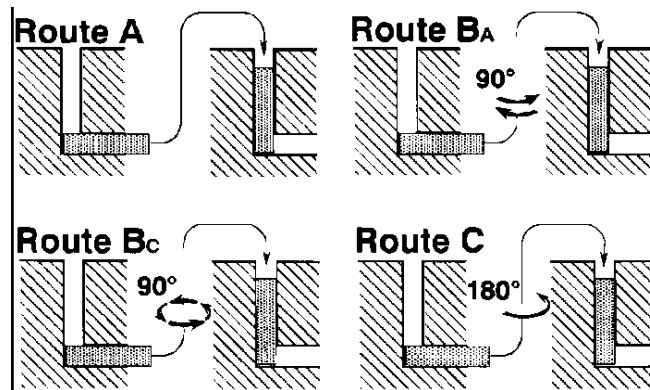


Figure 2.6 Four fundamental processing routes [50].

There are alternative multi-pass systems in ECAP process. During re-feeding of the material, rotating angles are given in Table 2.1 [51]. B_C is the optimum route to achieve super plasticity in the as-pressed condition. Furthermore, it leads to an array of equiaxed grains with high angle grain boundaries [52].

Both die and feeding parameters are the working subjects which are mainly focused on. These works include finite element method and aim to determine optimum die parameters [53-55].

Table 2.1 Rotation angles and directions for possible routes [51].

Route	Number of pressings						
	2	3	4	5	6	7	8
A	0°	0°	0°	0°	0°	0°	0°
B _A	90° ↙	90° ↘	90° ↙	90° ↘	90° ↙	90° ↘	90° ↙
B _C	90° ↙	90° ↙	90° ↙	90° ↙	90° ↙	90° ↙	90° ↙
C	180°	180°	180°	180°	180°	180°	180°
B _A -A	90° ↙	0°	90° ↘	0°	90° ↙	0°	90° ↘
B _C -A	90° ↙	0°	90° ↙	0°	90° ↙	0°	90° ↙

2.3.1 Parameters affecting ECAP Process

The *channel angle* Φ which is generally in the range of 90° to 120° is the most affecting parameter since the total strain imposed on the specimen is reversely proportional with the angle [4]. According to the experiments of Nakashima and his coworkers, optimum conditions are obtained to achieve ultra fine grain with high angle grain boundaries when Φ is close or equal to 90°. At these conditions a large plastic strain is imposed on the material in each pass through the die. Moreover, ~1 true strain is introduced on the material upon single pass [56].

The *arc angle* Ψ is the outer arc of curvature at the intersection of two channels constructing the die and it has inferior effect on the imposed strain value. The maximum load necessary for ECAP diminishes with a decrease in die outer arc angle [57].

Both of the channel angle Φ and the arc angle Ψ is illustrated in Figure 2.7.

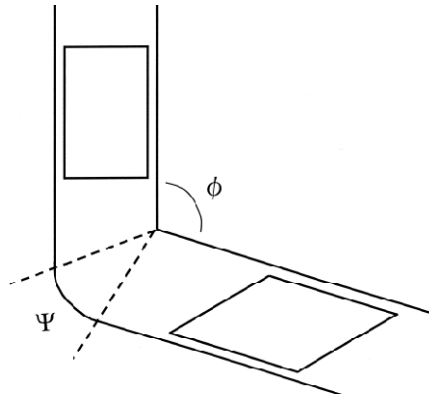


Figure 2.7 Schematic illustration of the ECAP die showing the channel angle Φ and the arc angle Ψ [12].

Previous studies show that as the *pressing temperature* increases, larger grains were obtained in pure Al, Al-Mg alloys and Al-Mg-Sc alloys. In addition, recovery rate increases at the higher pressing temperatures and this increases the chance of dislocation annihilation within the subgrains rather than being absorbed at the subgrain walls. This implies the difficulty of the evolution of the microstructure into an array of high angle boundaries at the higher pressing temperatures. So, retention of the subgrain structure is favored to higher total strains in pure Al during high temperature ECAP processes [58]. 2219 Al-alloy was subjected to ECAP process at temperatures in the range of 250°C and 475°C and it was concluded that subgrain formation is observed inside the deformation bands that are parallel to the pressing direction with an increase in the temperature [59]. 6061 Al-alloy was pressed both at 260°C, it was claimed that the micrograph consisted of well defined grain boundaries with low density of dislocations inside the grains [60].

Pressing speeds generally change from 1 to 20 mm/s when the high capacity hydraulic press is used in the construction [12]. In the study of Yamaguchi and his coworkers, 0.18 and 18 mms^{-1} pressing speeds were compared and it was concluded that the pressing speed has no significant effect on final microstructure of the Al-alloys [61].

Backpressure provides multi-pass operations without cracking. Although at low strains cracks are observed in the absence of backpressure, no cracking is observed at high strain values when the backpressure is applied. The workability of the material can be increased when the amount of backpressure is increased [62]. Backpressure can be applied both by another piston exerting at the end of the exit channel under computer control and measurement illustrated in Figure 2.8 [62] and by constructing a new die that consist of an exit channel with sliding bottom floor (unlubricated) which creates a friction and leads to backpressure [63].

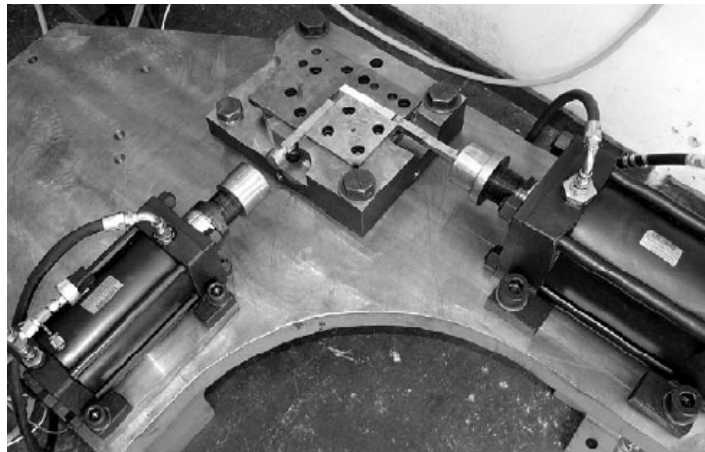


Figure 2.8 ECAP die with controlled backpressure [62].

2.3.2 Advantages of ECAP over Conventional Deformation Methods

Mainly, the process is applicable to the bulk billets which can be used in some of the structural applications and reasonable homogeneity can be acquired in most of the specimens after pressing. Moreover, the procedure can be performed easily once the die is constructed and applied to many materials such as several alloys including precipitation-hardened ones, steels, intermetallics, metal–matrix composites and so on [12].

There is a large increase in the strength especially in age hardenable alloys after ECAP in comparison with conventional deformation methods in the range of 18-36% and 16-28% in yield stress and tensile strength, respectively [64].

The sample is strained by shear during the deformation. The subgrain boundaries develop into high-angle boundaries by absorbing the dislocations so ultrafine grained structures separated by high-angle grain boundaries are achieved after ECAP due to the application of very high strain. In contrast, low angle to high angle grain boundary conversion cannot be achieved in conventional deformation methods because of the natural limit in the applied strain during deformation [50]. In addition, it is considered that the formation of fine-grained structures having high angle boundaries leads to the retention of ductility. When cold rolling and ECAP process are compared, it can be concluded that ECAPed specimens will have higher ductility values when the same strain is imposed on the specimens [19, 65]. For instance, if the cold rolling and ECAP processes are compared, it is apparent that the yield strength of 3004 Al-alloy increases with the increasing imposed strain by either cold rolling or ECAP. However, the ductility (elongation to failure) behaves in different manner after two processing methods. The ductility of the alloy decreases from ~32% to ~14% after one ECAP pass and no additional reduction in the ductility is observed with additional ECAP passes whereas cold-rolling decreases the ductility by a similar magnitude initially but then the ductility continues to decrease with increasing rolling strain even though at a slower rate (Figure 2.9) [66].

Another comparison of conventional metal-working and ECAP process is the consumption of the energy. The total work can be defined as the sum of "ideal work", "redundant work" and the work which is converted to heat and friction. The ideal work is the work required for macroscopic shape change that is due to the homogeneous plastic deformation whereas the redundant work is the corresponding amount of work due to shear processes which does not contribute directly to the external form of the product [67]. In conventional deformation methods such as rolling, extrusion there is a dimensional shape change in which the aim is to convert work to the shape change and some of the dislocations are used for the shape change. However, in ECAP process there is no change in dimensions meaning that there is no macroscopic shape change and in other words ideal work is zero. The energy is just used in internal shearing by dislocation creation and movement.

Thermal stability that is the resistance to grain growth after ECAP is another advantage of the process. No change in the grain sizes of 1100, 3004, 5083 and 6061

Al-alloys was observed up to an annealing temperature of 200°C after ECAP that can be seen in Figure 2.10 [65]. Detailed literature review about the thermal stability is given in part 2.4.2.

High angle grain boundaries contain large areas of poor fit and have a relatively open structure and the bonds between the atoms are broken or highly distorted and consequently the boundary is associated with a relatively high energy [68]. High energy and non-equilibrium state after ECAP can be the reason of thermal stability. To conclude, ECAPed specimens have resistance to grain growth during annealing due to the high angle grain boundaries and it is predicted stable microstructures are achieved by high angle grain boundaries [69]. If the same annealing procedure has been applied to ECAPed and conventionally deformed specimens, the ECAPed one will have higher strength due to the high dislocation density. Resistance of ECAPed specimen to grain growth during annealing is higher than the conventionally deformed one. This stems from the high energy dislocations at the grain boundaries.

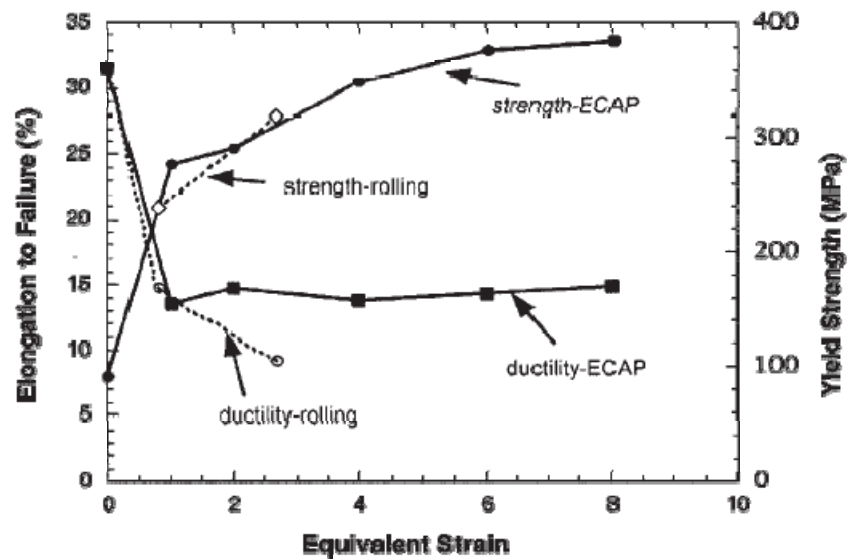


Figure 2.9 Comparison of yield strength and ductility of ECAPed and cold-rolled 3004 Al-alloy [66].

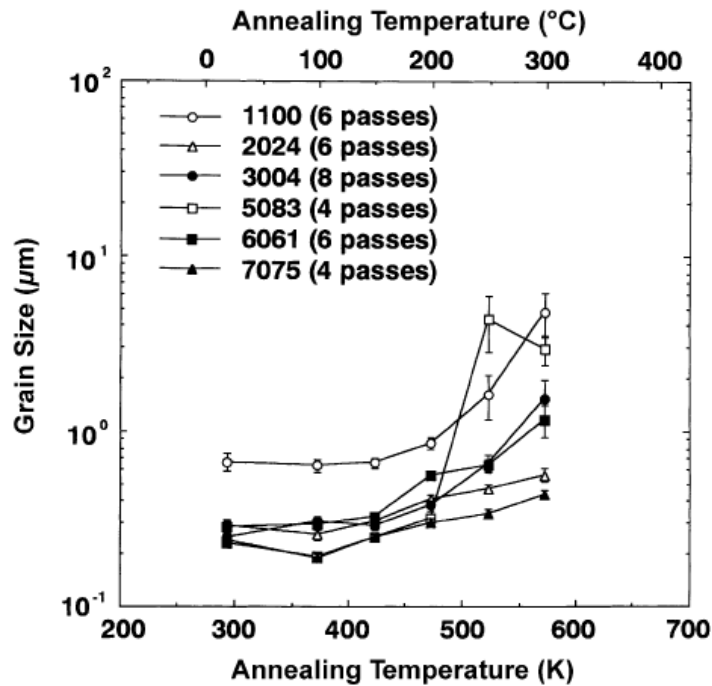


Figure 2.10 Variation of grain size with annealing temperature for various Al-alloys [65].

2.3.3 Microstructural and Mechanical Improvement by ECAP

In some Al-alloys boundaries are not defined well after ECAP whereas some of them show boundaries well that prove the grain refinement. Hardness and UTS increases especially after one pass but ductility decreases and remains constant generally after one-pass ECAP. When 1100, 2024, 3004, 5083, 7075 were subjected to ECAP, high angle grain boundaries are determined due to the SAED patterns and dislocations were observed inside the grains surrounded by wavy boundaries which cannot be defined easily [65]. Moreover, in the ECAPed 6061 Al-alloy, the boundaries were ill-defined with a high dislocation density inside the grains seen in Figure 2.11 and ill-defined grain boundaries were attributed to the presence of high-energy non-equilibrium boundaries [60, 65].

Kim et al. claimed that curved or wavy grain boundaries are seen in 2024 Al-alloy specimen after one pass, that are corrugated with regular or irregular arrangement of facets or steps and spread grain boundary contours indicate that grain boundaries are

in a relatively high energy and non-equilibrium state as in other ECAPed materials [70]. One-pass ECAPed Al-1.7 at% Cu alloy has a microstructure consisting of subgrain bands with a spacing of 100-500 nm and tangled dislocations. The subgrain size was in the range of 100-500 nm in the longitudinal direction and the size was almost equal to shear band size in the transverse direction (Figure 2.12). Upon further ECAP passes, fine equiaxed subgrains were acquired and subgrain sizes were determined as 300nm after three passes and 100nm after five passes [71]. Similarly, in the study of Kim and his coworkers, elongated subgrain bands were appeared in the 6061 Al-alloy after one pass ECAP and equiaxed subgrains were formed after four passes with the subgrain size of 0.3-0.4 μm [72].

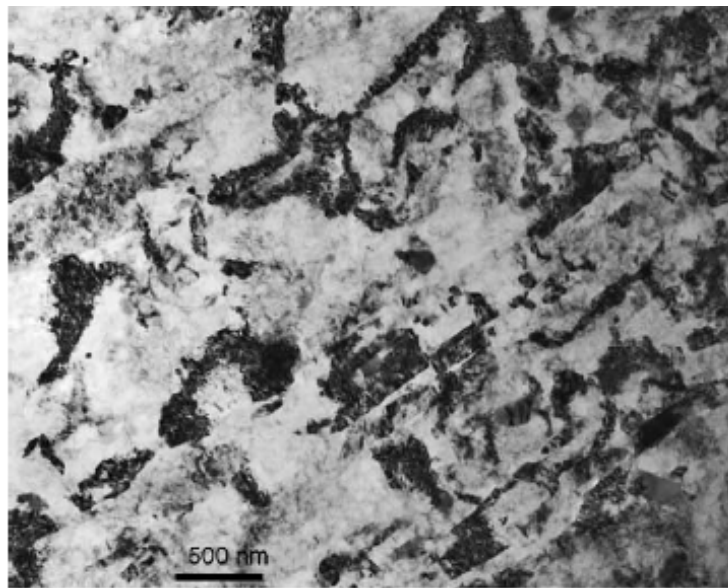


Figure 2.11 TEM micrograph of ECAPed 6061 Al-alloy [60].

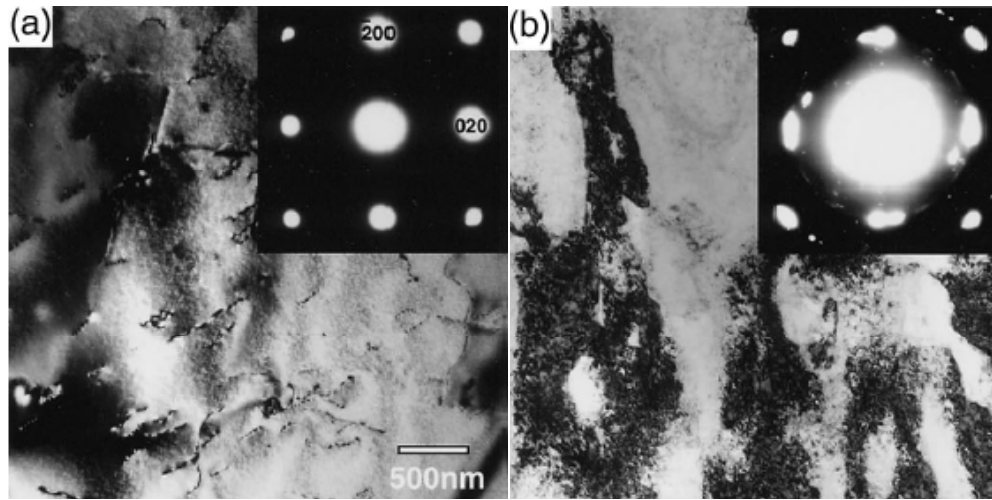


Figure 2.12 TEM micrographs and corresponding SAED patterns of **a.** unECAPed **b.** one- pass ECAPed single phase Al-1.7 at% Cu alloy [71].

Ultra fine grain sizes can be achieved via ECAP processing and can be observed in some Al-alloys if the boundaries are seen clearly. The grain refinement was observed in the four pass ECAPed Al-0.63%Cu alloy down to submicron levels and the grain size was decreased to 200-300 nm in ECAPed Al-3.9%Cu alloy [73].

In the study of Cheng and his coworkers, the importance of remained T-phase dispersoids in grain size reduction and dislocation pinning upon deformation was emphasized. In Figure 2.13 gathered dislocation cumulus around the dispersoids during cyro-rolling of 2024 Al-alloy at a temperature below $-150\text{ }^{\circ}\text{C}$ and dislocation cumulation due to increase in imposed strain can be seen sequentially. Figure 2.13 (a) shows dislocation tangling at a strain of $\sim 15\%$ and (b) shows increased dislocation density between the dispersoids and low density of dislocations in the regions without dispersoids when $\sim 40\%$ strain was reached. Moreover, in Figure 2.13 (c) homogeneous distribution of dislocations were seen at a strain of $\sim 80\%$ [11].

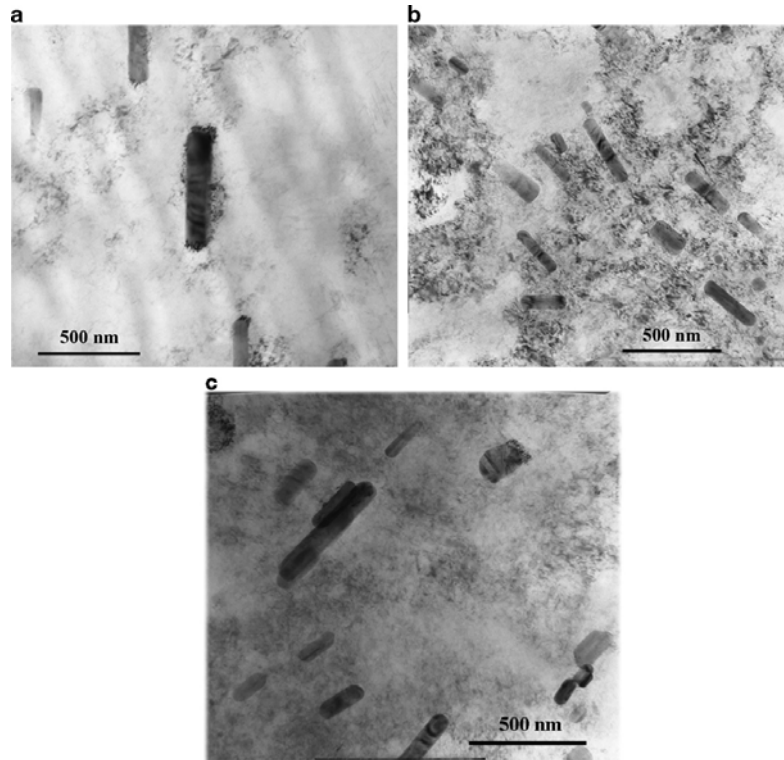


Figure 2.13 Dislocation tangling after cyro-rolling of 2024 Al-alloy at a strain of **a.** ~15% **b.** ~40% **c.** ~80% [11].

When the solutionized Al-1.7 at% Cu alloy was subjected to ECAP, the hardness of the specimen was increased up to value that is 80% of the total increase after only one pass [71]. Similarly, 55% increase in hardness was detected after one pass while four passes lead to an increase of 85% [72] designated in Figure 2.14. Similarly, there is a significant increase in strength after one pass in 2024 Al-alloy. Kim and his colleagues emphasized on another advantage of post-ECAP aging which is the ability to optimize ductility and strength in 2024 Al-alloy. Yield strength of the ECAPed specimen was reached to 570MPa that is 72% higher than that of the unECAPed one which is 330 MPa (Figure 2.15) [70]. There was a significant increase in the proof stress up to a point corresponding to one equivalent strain and further increase in strain resulted in a gradual increase in the stress seen in Figure 2.16. Highest proof stress was obtained in 5083 whereas lowest was found in 1100. In contrast, the elongation to failure decreased very much after one pass. The elongation to failure did

not change with further increase in the strain but increased in 5083. It is suggested that the toughness increased after ECAP [65].

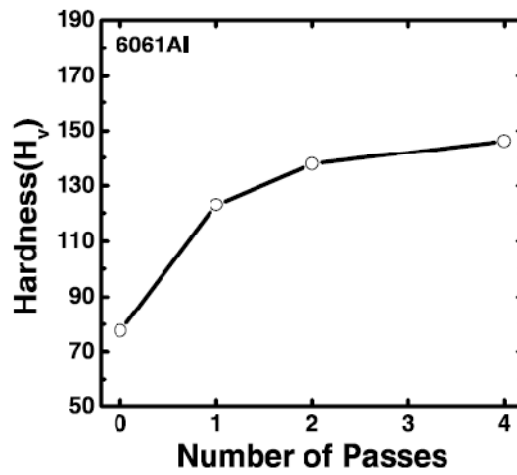


Figure 2.14 Vickers' hardness versus number of ECAP pass in 6061 Al-alloy [72].

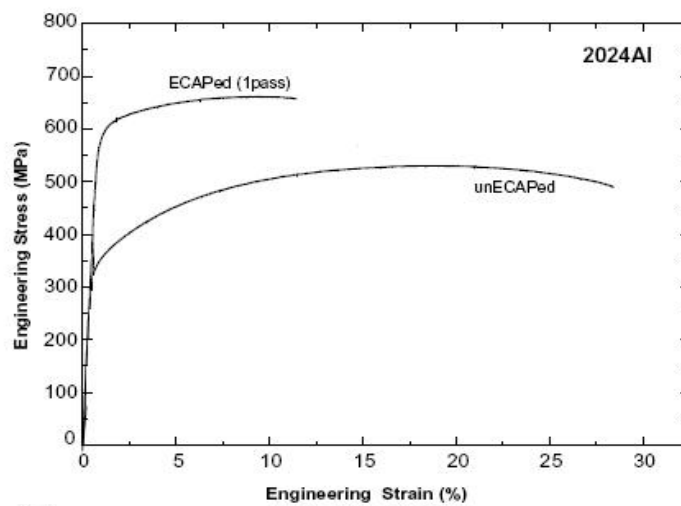


Figure 2.15 The stress–strain curves of the unECAPed and ECAP processed 2024 Al alloys [70].

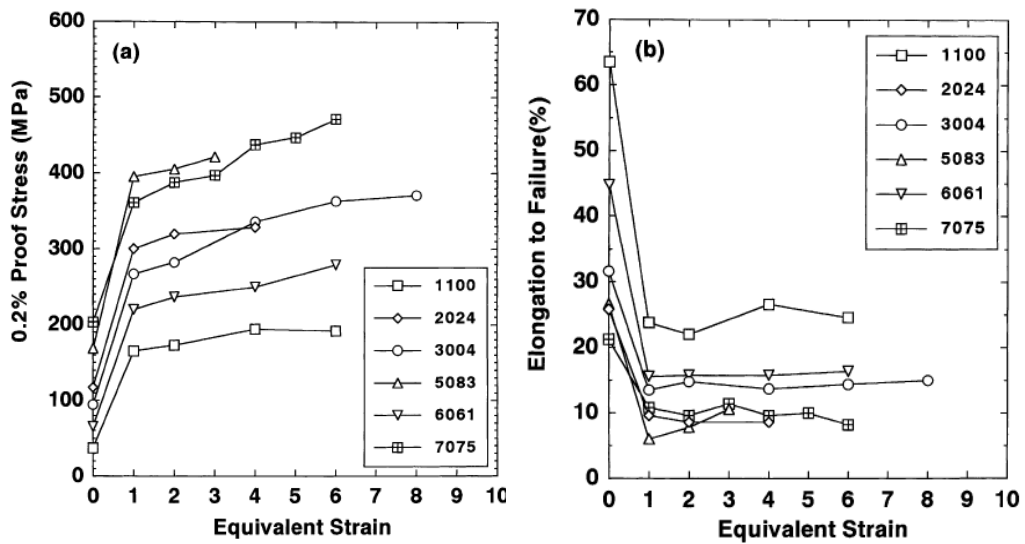


Figure 2.16 a. 0.2% proof stress b. elongation to failure versus equivalent strain graphs of various Al-alloys after ECAP [65].

It has also been reported that the elongation of Al-0.63% Cu alloy is superior to that of Al-3.9% Cu alloy whereas the strength of the previous one is lower than that of the following alloy. Moreover, after six pass ECAP process there was an increase in the UTS value of Al-0.63% Cu alloy from 83 MPa to 239 MPa due to strain hardening and a decrease in the elongation after one pass ECAP but no change was observed in elongation upon further passes. Similarly, UTS was increased up to 207 MPa in one pass ECAPed Al-3.9% Cu alloy and to 290MPa after four passes. The elongation decreased from 7.8 to 1.5% after one pass but it increased with the number of further passes and finally reached to 2.7% after four passes [73].

2.4 Heat Treatment after ECAP

2.4.1 Age Hardening

There are studies to determine the best combination of the age hardening treatment and ECAP process in strengthening the alloys. In the study of Mao and his coworkers,

“solutionizing+aging+ECAP” combination was chosen so the solutionized 2024 Al-alloy specimens were peak-aged (PA) at 190°C for 16h and over-aged (OA) at 290°C for 1h then the specimens were subjected to ECAP at 190°C and 150°C, respectively. The grains have high density of dislocations that were surrounded by undefined and wavy boundaries shown in Figure 2.17 (a) and (c). Furthermore, the SAED pattern demonstrated that the fine grains were distinguished by high angle grain boundaries [38].

According to the study of Zheng and his colleagues, four types of ECAP and heat treatment combinations (Table 2.2) were compared in 7050 Al-alloy and 4th condition was selected as the best in obtaining finer grains and higher strength that the ultimate tensile strength of the alloy reached to 677MPa after 3-pass ECAP that is 30% more than that of T6 conditioned material. In addition, conditions were listed from 4 to 1 in the descending order of strength sequentially. TEM micrographs of 7050 Al-alloy at four conditions were given in Table 2.2. In condition 1 the width of shearing bands decreased to 4-5 μm after four passes of ECAP since the width of shear bands decreases with the number of ECAP passes. In condition 2, coarse shear bands were replaced by the fine grains with less than 1 μm size that are surrounded by defined grain boundaries. The formation of fine elongated grains can be attributed to recrystallization during short annealing treatment that lead to decrease in internal elastic stress and defect annihilation partially [74].

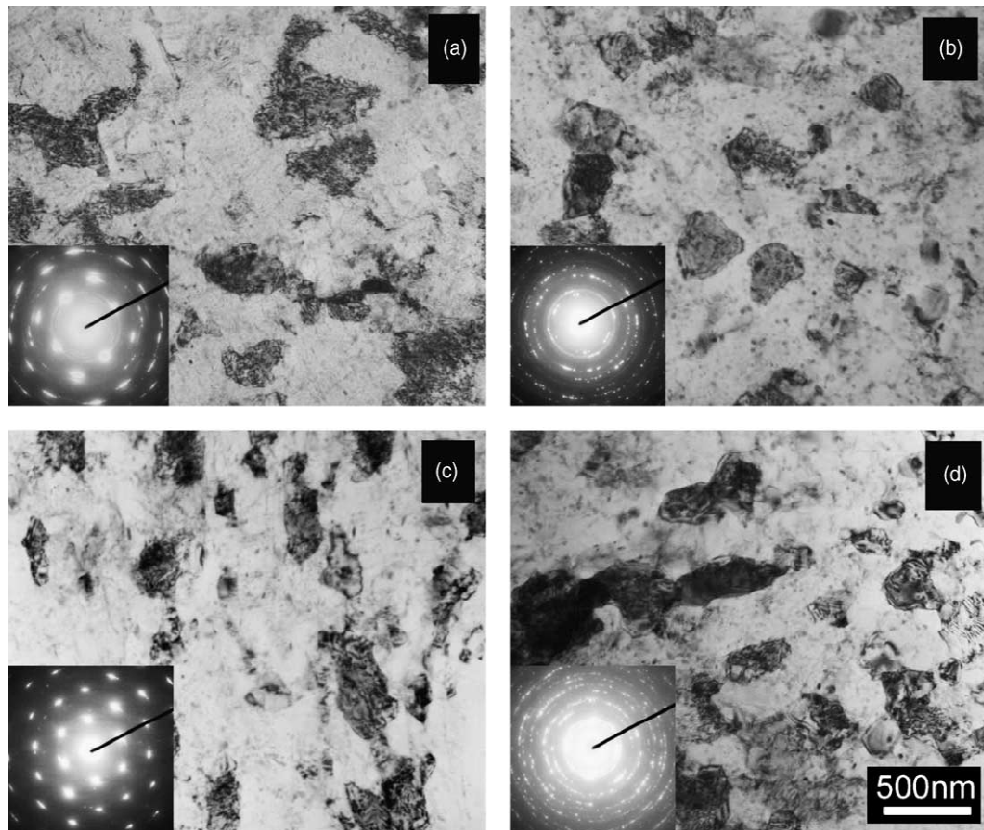
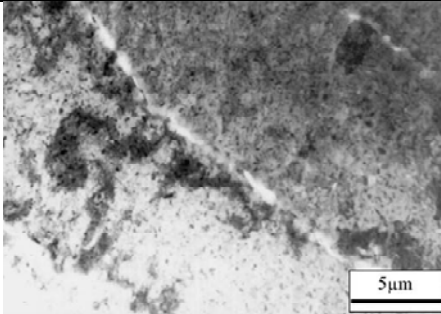
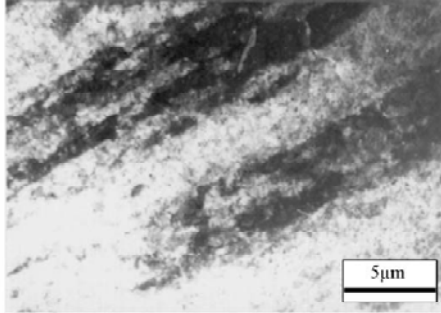
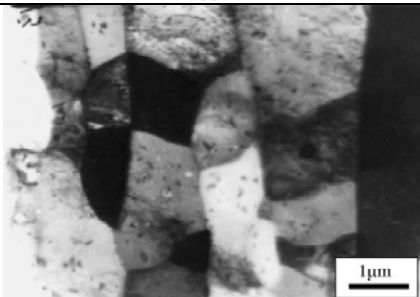
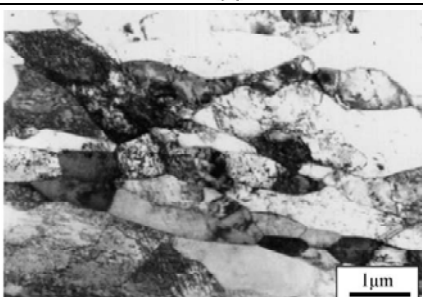
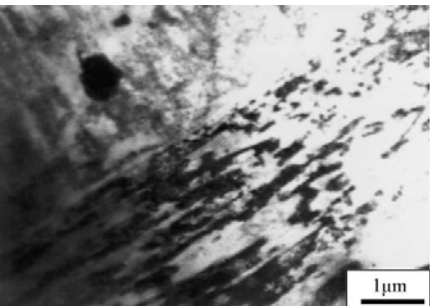
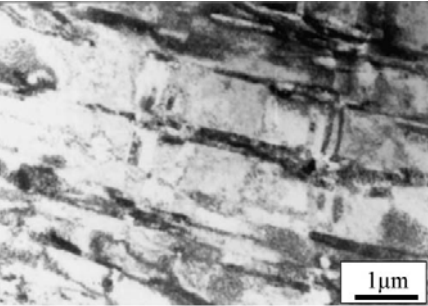
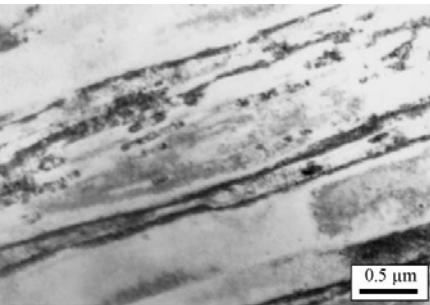
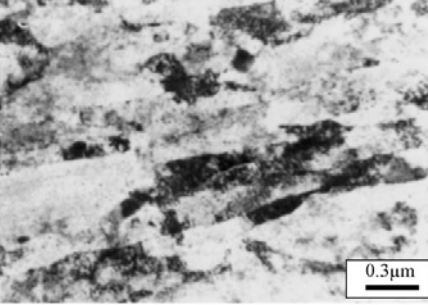


Figure 2.17 TEM micrographs and corresponding SAED patterns of 2024 Al-alloy **a.** PA specimen after two passes **b.** PA specimen after eight passes **c.** OA specimen after two passes and **d.** OA specimen after eight passes [38].

Thin shear bands were produced in condition 3 with a different morphology than the ones observed in condition 1. Uniform shear bands appeared after one pass ECAP in condition 4 and fine grains aroused along the bands with an average grain size of 300nm with a highest grain refinement rate [74].

In another study, two routes of “solutionizing+ECAP+aging” combination [75] were compared in 6061 Al-alloy. Route 1 was “solutionizing + water quenching + ECAP + aging (WQ-ECAPed)”, and route 2 was “solutionizing + furnace cooling + ECAP + aging (FC-ECAPed)”. Higher density of dislocations was observed in the WQ-ECAPed specimen. Moreover, corresponding SAED patterns in the figure pointed to presence of higher number of small subgrains having higher grain boundary misorientation angles in WQ-ECAPed as compared to FC-ECAPed specimen (Figure 2.18) [75].

Table 2.2 TEM micrographs of 7050 Al-alloy for 4 different conditions [74].

	After 1 pass	After 4 passes
Condition 1	 (a)	 (b)
Condition 2	 (a)	 (b)
Condition 3	 (a)	 (b)
Condition 4	 (a)	 (b)

- Condition 1* Annealing (280°C)+ECAP+Aging(120°C)
Condition 2 Annealing (280°C)+ECAP+Annealing (470°C)+Aging (120°C)
Condition 3 Annealing (280°C)+ECAP+Annealing (470°C)+ ECAP+Aging (120°C)
Condition 4 Solutionizing (470°C)+ECAP (120°C)+ Aging (120°C)

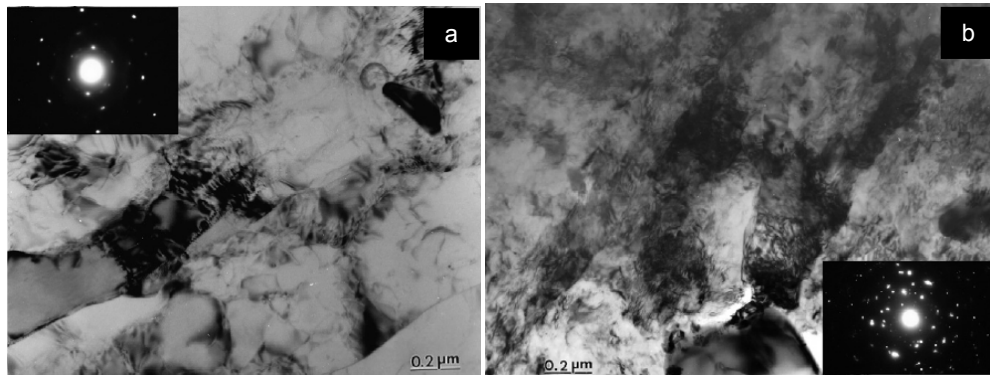


Figure 2.18 TEM micrograph and corresponding SAED patterns of 6061 Al-alloy [75]
a. FC-ECAPed and **b.** WQ-ECAPed 6061 Al-alloy.

By using the “solutionizing + ECAP + aging” combination it was determined that the precipitation kinetics is accelerated by prior ECAP process without change in the precipitation sequence in 7075 Al-alloy [30]. When the hardness profiles of the ECAPed and unECAPed 2024 Al-alloy specimens were compared at constant temperature, it is seen that the profile of the ECAPed one shifted to shorter times as shown in Figure 2.19 (a). Another important point is the aging temperature determination. During post-ECAP aging treatment of 2024 Al-alloy, it is seen from Figure 2.19 (b) that at higher aging temperature (448 K) peak hardness was achieved at lower times [70]. However; if the aging temperature is high, there will not be an increase in strength due to the annealing effect so the temperature must be kept at low temperatures like 100-110 °C to have best aging effect on strengthening [36, 64, 72, 76]. ECAPed 6061 Al-alloy displayed an increase in hardness especially at lower number of passes in Figure 2.20 (a) but much higher raise was seen in the unECAPed one at 175 °C. On the other hand, at an aging temperature of 100 °C significant hardness increase in ECAPed specimens were displayed in Figure 2.20 (b) since the softening effect is overwhelmed by the age hardening effect [72]. The consistency of hardness data given in Figure 2.20 and the engineering stress-strain curves of the ECAPed, ECAPed+aged and unECAPed 6061 Al-alloy specimens given in Figure 2.21 that shows the increase in tensile strength of ECAPed+aged specimen was achieved. In comparison with the peak-aged unECAPed specimen, ~40% increase in UTS and yield strength was obtained (Figure 2.21) [72].

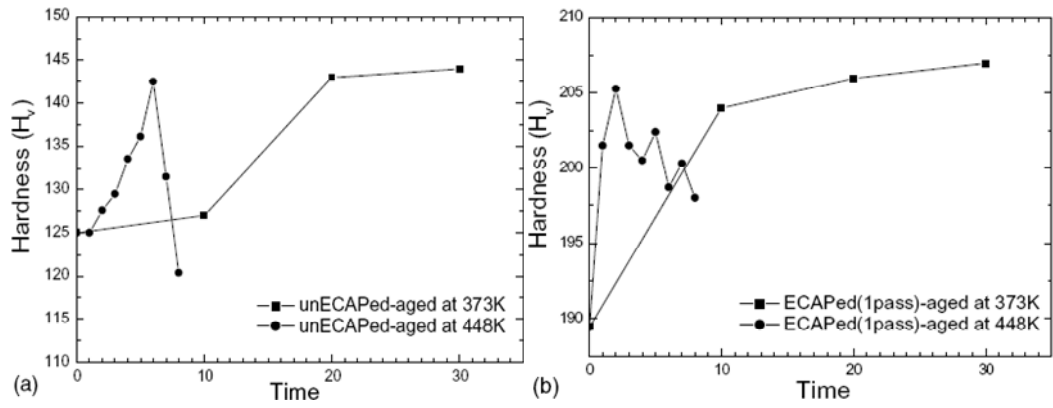


Figure 2.19 Age hardening profiles of **a.** unECAPed and **b.** ECAPed 2024 Al-alloy specimens aged at 100 °C and 175 °C [70].

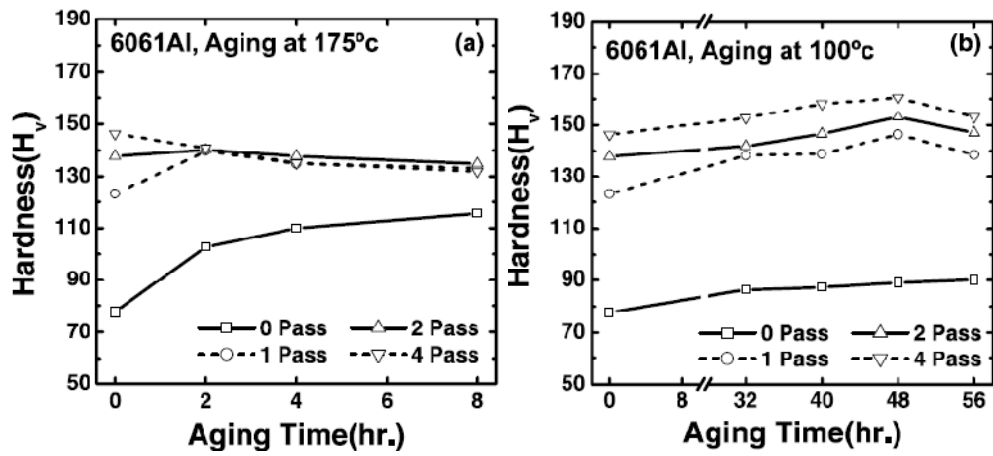


Figure 2.20 Age hardening profiles of ECAPed and unECAPed 6061 Al-alloy specimens **a.** at 175 °C **b.** at 100 °C [72].

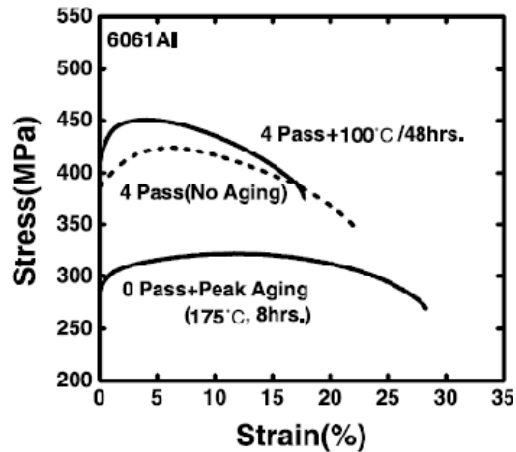


Figure 2.21 Stress-strain curves of only peak aged (175 °C, 8h), 4-pass ECAPed+peak aged (100 °C, 48h) and only ECAPed 6061 Al-alloy specimens [72].

In contrast with the previous study, a slight decrease in strength was observed in the AlMgSi alloy (6082) whereas an increase in ductility was designated with post-ECAP aging process at 90-130 °C in Figure 2.22 (a). Figure 2.22 (b) shows the effect of age hardening treatment on hardness of ECAPed and unECAPed alloy. In the unECAPed alloy, typical age hardening curve was obtained at an aging temperature of 110 °C but swift softening was discerned at 175 °C in Figure 2.22 (b). On the other hand, minor increase in hardness was achieved with post-ECAP aging at both aging temperatures and shifting to shorter times was observed in the age hardening profile as the aging temperature increased due to the increase in age hardening kinetics shown in Figure 2.22 (b) [64].

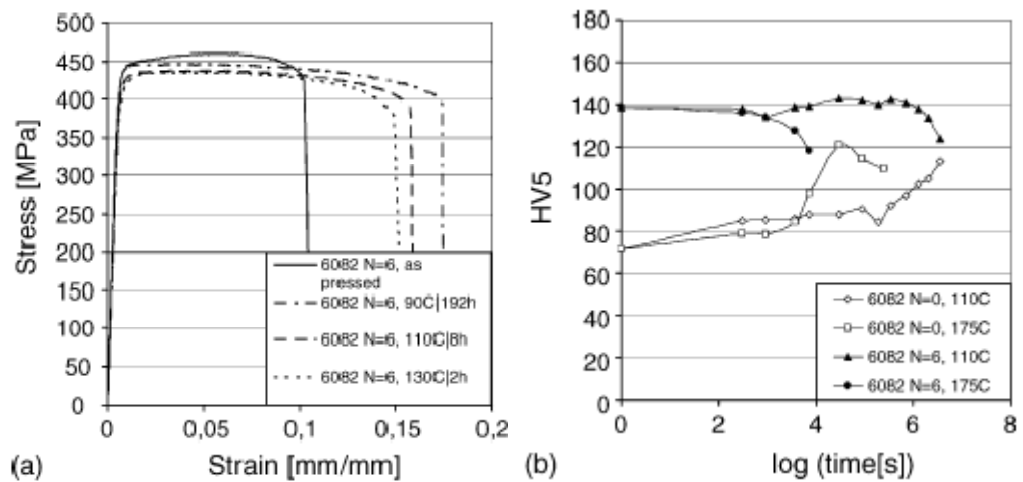


Figure 2.22 a. Effect of aging temperature on strength and ductility in 6-pass ECAPed AlMgSi alloy **b.** Age hardening profiles of ECAPed and unECAPed alloys at 110 and 175 °C [64].

It can be concluded that there are mainly four advantages of post-ECAP low temperature aging; firstly the ability of the solutionized matrix to have an increased rate of dislocation accumulation, secondly inhibition of the breaking down of the pre-formed precipitates during ECAP, thirdly elimination of the recovery by precipitation on the ECAPed structure and decreasing the aging temperature and finally increase in the aging kinetics at low temperatures due to the high dislocation density in the ECAPed structure [72].

The presence of the pre-precipitates or the precipitates after post-ECAP aging process was designated in TEM micrographs [70-72]. In 6061 Al-alloy, high density of spherical and fine precipitates with the diameter of ~20 nm were formed during aging at 100 °C for 48h and these precipitates were located at the preferable places where dislocations accumulate during deformation that can be seen in Figure 2.23. The typical size of the GP zone was smaller than the spherical precipitates observed in Figure 2.23 and the reason can be attributed to the increase in diffusion and stress field due to the large increase in dislocation density and other defects [72].

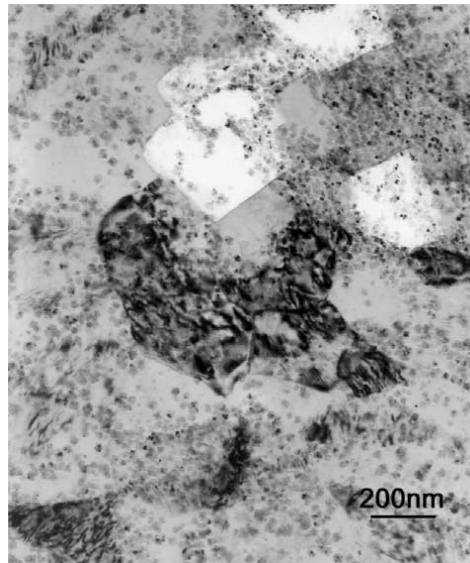


Figure 2.23 TEM micrograph of four pass ECAPed and aged (100 °C / 48h) 6061 Al-alloy [72].

Figure 2.24 (a) shows the TEM micrograph of the unECAPed Al-Cu alloy that was aged at 100 °C for 24h showing the uniformly dispersed GP zones with a diameter of ~20nm. GP zone density decreased in the one pass ECAPed + aged (100 °C for 24h) shown in Figure 2.24 (b) that denotes the GP zone formation was extinguished by severe plastic deformation. Furthermore, heterogeneous nucleation of θ' precipitates were discerned at the nucleation sites which are dislocations formed by ECAP. Pre-precipitates such as GP zones, θ'' , θ' phases were not observed in the TEM micrograph of eight pass ECAPed + aged (100 °C for 24h) given in Figure 2.24 (c) but the evidence for the equilibrium precipitate θ presence was marked by the arrows in the corresponding SAED pattern. Figure 2.24 (d) shows the dark-field image of the same material displaying the θ precipitates at the grain boundaries. So it can be deduced that decreasing the grain size changes the sequence of precipitates, in other words, the stable precipitate can be formed at the beginning without formation of pre-precipitates due to the decrease in grain size [71].

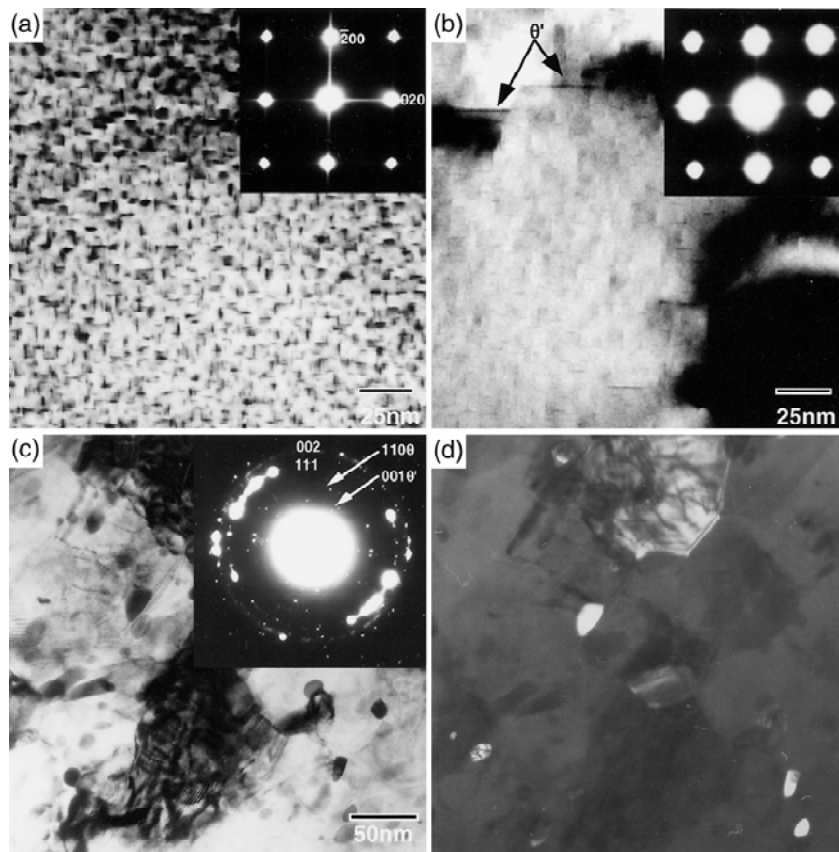


Figure 2.24 Bright field TEM images and corresponding SAED patterns of **a.** aged (100 °C, 24h) **b.** one pass ECAPed + aged (100 °C / 24h) **c.** eight pass ECAP + aged (100 °C / 24h) **d.** Dark-field image of eight pass ECAP + aged (100 °C / 24h) of Al-1.7at% Cu alloy [71].

Precipitates were exhibited in the TEM micrographs (Figure 2.25) of the ECAPed + aged (100°C / 20h) 2024 Al-alloy specimen. Figure 2.25 (a) shows the high density of dislocations and needle-like, small precipitates that were located around the dislocations. The precipitates are seen as white in the dark field image and marked with arrows in the figure. In addition, it was not decided that the observed precipitates are S' (Al₂CuMg) that are formed generally in Al-Mg-Cu alloys because the aging temperature (100 °C) was lower compared to the usual aging temperatures (170-180 °C). Precipitates seen in the figure were not large in size and this can be due to the low aging temperature and high density of dislocations that serve as nucleation site for the precipitates. Moreover, Figure 2.25 (b) shows the morphology and distribution of the equilibrium S precipitate in 2024 Al-alloy [70].

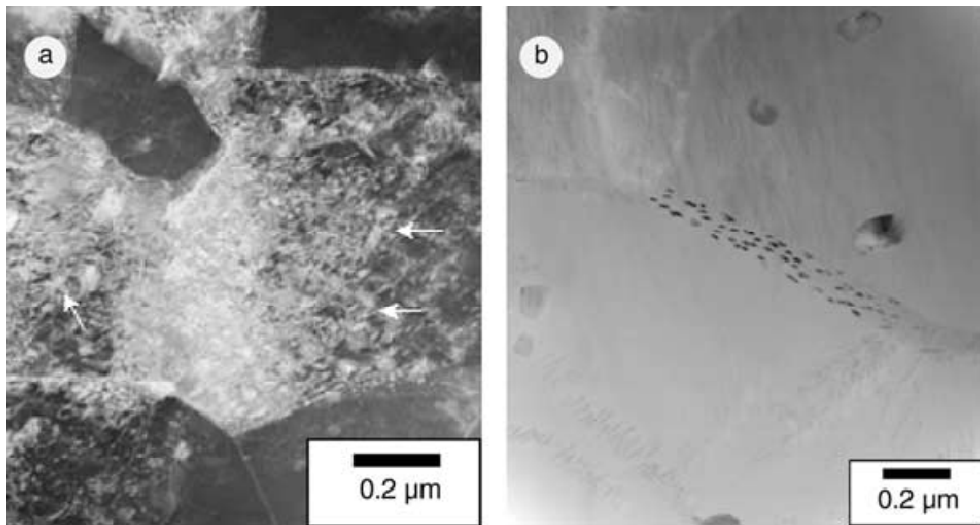


Figure 2.25 TEM micrographs of the ECAPed + aged (100°C / 20h) 2024 Al-alloy
a. low magnification, **b.** high magnification [70].

2.4.2 Annealing

When the deformed metal is heated at a temperature of one-half of its melting point and is hold at this temperature, up to time t_1 recovery stage is occurred. At time t_1 nucleation of new grains within the cold-worked grains of the matrix is observed and these grains then grow rapidly until all of the cold-worked grains were gone at time t_2 . These new grains then grow slowly until at time t_3 a final grain size is obtained.

During recovery stage, rearrangement of dislocations within tangles, annihilation of dislocations and subgrain growth occur.

Metals with wide stacking faults (low stacking fault energy) such as Al, Cu, Ni, Au strain-harden more rapidly, twin easily on annealing than metals with narrow stacking faults. Moreover, in metals with high stacking fault energy (SFE) dislocation tangles and cells are formed upon deformation, whereas in low stacking fault energy metals banded structure and linear arrays of dislocations constitute the structure [2]. When aluminum is deformed at room temperature distinct subgrain or cell structure is formed since high stacking fault energy of aluminum does not impede cross slip. If distinct dislocation tangles do not occur in a metal after deformation yet, they will be formed

upon annealing and defined subgrain boundaries will be formed by condensation of the tangles due to additional annealing as illustrated in Figure 2.26. These results show that the dislocation network can lower its energy by forming tangles rather than random arrays [77].

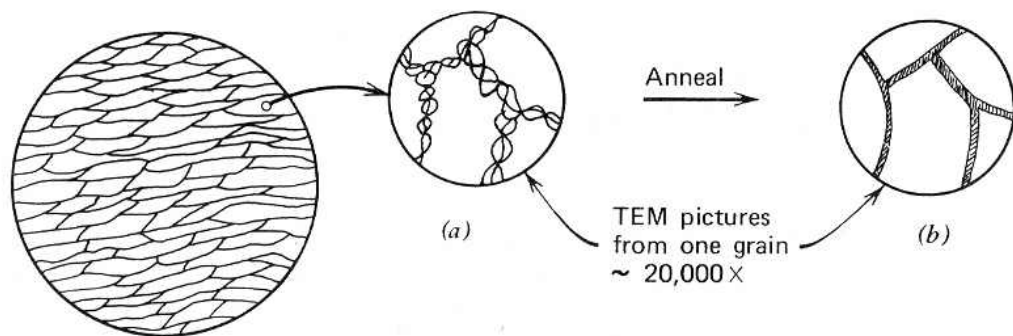


Figure 2.26 Schematic view of grain and subgrain (cell) structure in aluminum [77].

The same procedure is valid for deformation by ECAP. There are studies about post-ECAP annealing treatments showing thermal stability that is the resistance to grain growth upon annealing of ECAPed specimens. Four pass ECAPed 7050 Al-alloy specimens at room temperature has an average grain size of 660nm and even after annealing at 470°C for 0.5 h fine grains were maintained with a size less than 1 μm [78]. Furthermore, in the ECAPed Al-3Mg alloy with elongated grains about 0.1 μm in width and about 1-1.2 μm in length, slight coarsening was occurred and equiaxed grains were observed with grain sizes of 0.25 μm and 0.5-1 μm, respectively after annealing at 200°C for 1h and 250°C for 5-15 min whereas no significant change in the microstructure was seen at an annealing temperature of 150°C for 1h. However, duplex (recovered + recrystallized) structure and coarse grains with a size of 5-10 μm were obtained after an annealing treatment at 250°C for 1 h [79]. Furthermore, in Al-Zr alloys fine grained structure was retained even at 600K (327 °C) whereas in pure Al and Al-Mg alloys thermal stability was not retained at such a high temperature [80]. However, in pure Al, high angle grain boundaries that limit the grain growth were observed even after annealing at temperatures below 275°C [81]. To summarize,

annealing at high temperatures leads to subgrain refinement by subgrain formation initially by dislocation tangling then due to discontinuous recrystallization and subgrain growth which will lead to an increase in grain size [79, 82-84]. In addition, even at high annealing temperatures grain refinement can be maintained if particles were present that can impede grain growth [19, 85].

CHAPTER 3

EXPERIMENTAL PROCEDURE

In this chapter, first, the material used throughout the study, then experimental studies conducted on ECAP and then heat treatment (aging and annealing) studies prior to and after severe plastic deformation are given. Next, information about experimental set-up used in ECAP and heat treatment experiments are explained. At the end, characterization methods such as, X-Ray diffraction analysis, microstructural investigation (optical microscopy, SEM, TEM) and mechanical characterization studies are explained.

As it was represented in Figure 3.1, the solutionized specimens were age hardened before and after ECAP process to obtain hardness profiles. In addition, microstructural analysis was done for solutionized, solutionized + aged, solutionized + ECAPed, solutionized + ECAPed + heat treated like annealing and aging. Moreover, X-ray diffraction analysis was carried out for ECAPed and annealed specimens.

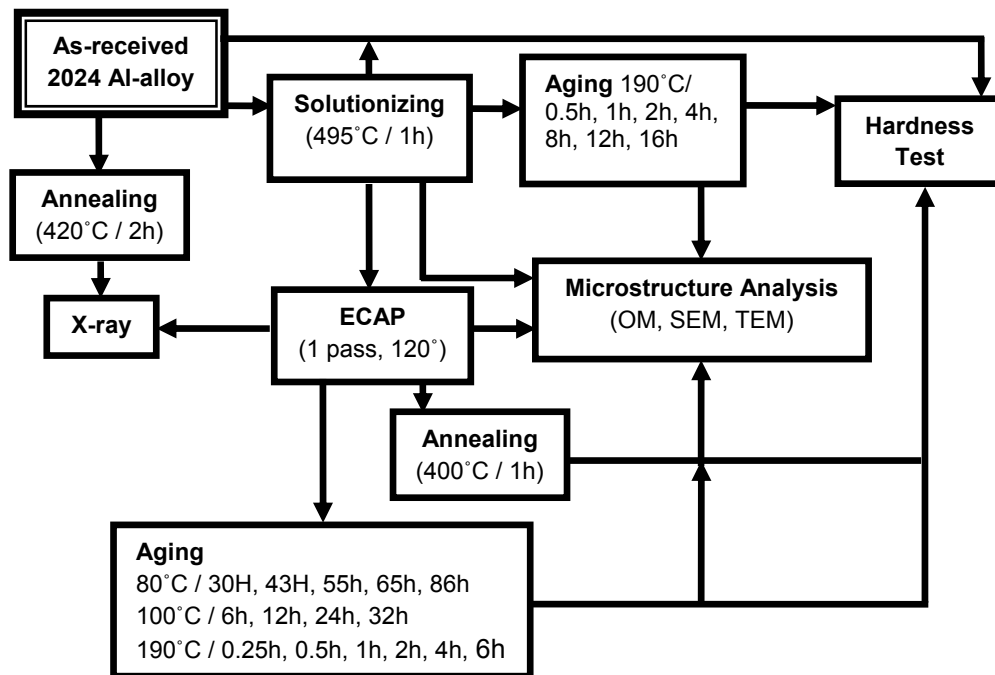


Figure 3.1 General experimental layout.

3.1 Material

In the preliminary studies, 6066 and 5058 Al alloys were used. Mainly 2024 Al-alloy was used throughout the study. The chemical composition of the 2024 Al-alloy was given in Table 3.1. This study was conducted using rectangular prism shaped specimens with dimensions of 14x14x10 mm and cylindrical specimens with 18 mm diameter and 10 mm length taken from 2024 Al-alloy.

Table 3.1 Comparison of the spectral analysis of the alloy used and standard 2024 Al-alloy.

	<i>Al</i>	<i>Si</i>	<i>Fe</i>	<i>Cu</i>	<i>Mn</i>	<i>Mg</i>	<i>Zn</i>	<i>Cr</i>	<i>Ti</i>
Used	92.6	0.106	0.217	4.9	0.595	1.24	0.156	0.0166 <	0.0292
Standard	90.7-94.7	<0.5	<0.5	3.8 - 4.9	0.3 - 0.9	1.20 - 1.80	<0.250	<0.100	< 0.150

3.2 Die Design

Preliminary studies were carried out to determine optimum process parameters since the final properties of the material were directly related to the channel angle, surface, design etc. of the die and also to the state of the material.

3.2.1. Initial Trials

First trials were carried out with the first ECAP system having vertical axis hydraulic press (Figure 3.2). The ECAP die with 90° channel angle consisting of two parts was made out of tool steel (Figure 3.3) was placed below the vertical axis hydraulic press. Although the press capacity was 30 tones, specimens were pressed approximately at 20 tones. Rubber was pressed from top of the die in order to push the specimen out. All of the specimens, rubbers and the die were lubricated with MoS₂.



Figure 3.2 Vertical axis hydraulic press with 30 ton capacity.



Figure 3.3 ECAP die with 90° channel angle.

Trial 1: Three 6066 Al-alloy specimens (14x14x130 mm) were passed through the die. The first specimen was cracked from several points. But, the cracks were observed only at the start and finish points of the pre-heat treated (at 450°C for 60h and 120h) since specimens were more ductile (Figure 3.4). Hardness values were determined along the bar from six points (Table 3.2).

Table 3.2 Hardness values of the 6066 Al-alloy samples.

Specimen	Average Hardness (HB)	Specimen	Average Hardness (HB)
As-received	67 ± 0.8	ECAPed	84 ± 12
Annealed (450°C / 60h)	56 ± 0.5	Annealed (450°C / 60h)+ ECAPed	84 ± 3.2
Annealed (450°C / 120h)	55 ± 1.2	Annealed (450°C / 120h)+ECAPed	85 ± 1.6

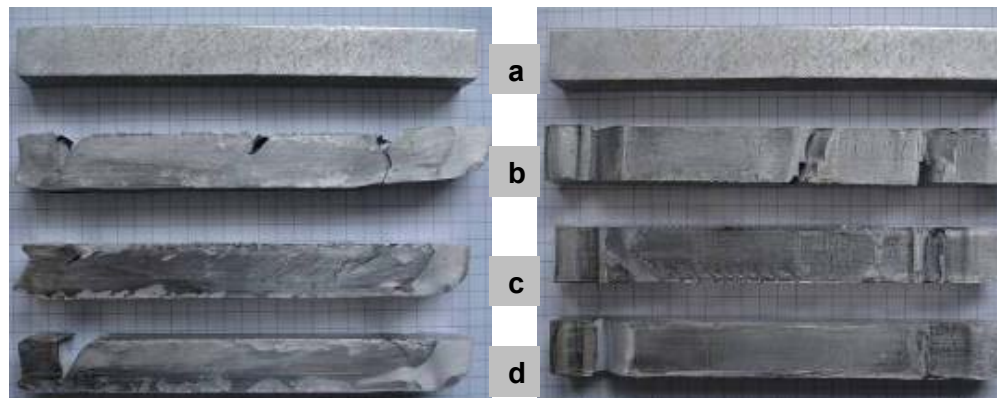


Figure 3.4 Two side views of (a) unECAPed (b) ECAPed without prior heat treatment (c) annealed at 450°C for 60h and ECAPed (d) annealed at 450°C for 120h and ECAPed specimens.

The hardness value (~67 HB) decreased initially due to the heat treatment, but after 72 h it became constant at about 52 HB as seen in Figure 3.5.

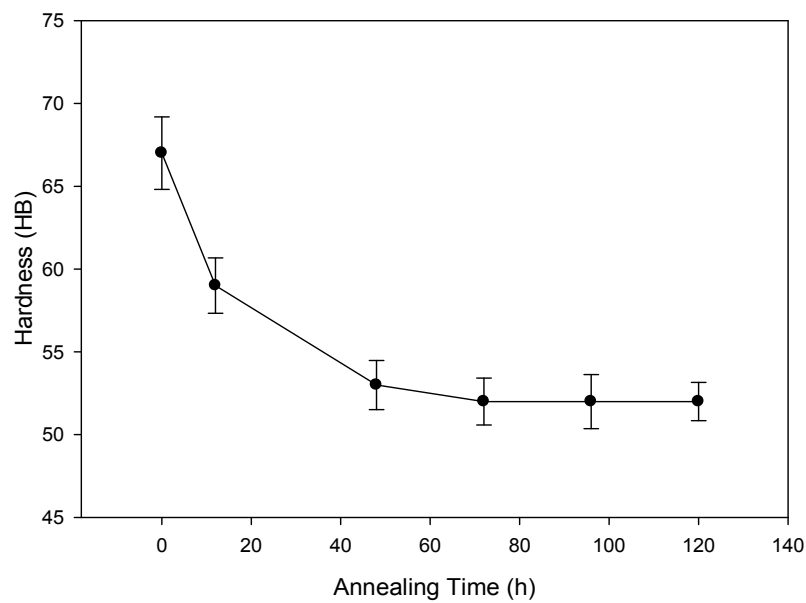


Figure 3.5 Variation of hardness in 6066 Al-alloy samples as a function of annealing time at 450 °C.

The hardness profile was obtained from a piece taken from the mid-point of the heat treated (450°C / 120h) specimen. In Figure 3.6, surface 1 was the upper, 3 was the lower and 2 was the lateral surface of the specimen. The effect of the deformation was remarkable in the perpendicular axis rather than horizontal axis seen in Figure 3.7.

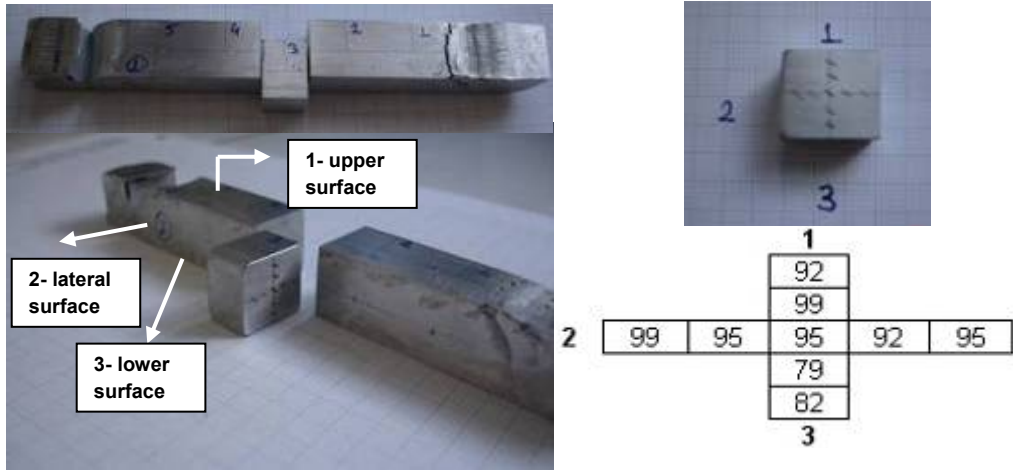


Figure 3.6 Coding of specimen surfaces.

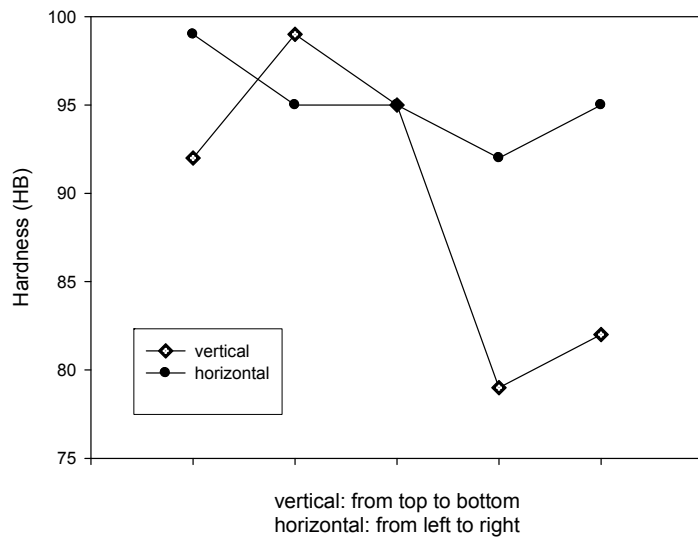


Figure 3.7 Hardness profile along the cross-section of 6066 Al-alloy after ECAP.

Trial 2: 5083 Al-alloy was used. One of the specimens was heated up to 415 °C for 144h at which the hardness became constant (Figure 3.8) before ECAP and the other one was used in the as-received condition. Cracks were observed in both heat treated and as-received specimens after ECAP. As seen in Figure 3.9 cracking occurred only at the tips in prior heat treated specimen while cracks were observed both at the tips and at the center in the as-received ECAPed specimens. Average hardness values of the specimens were given in Table 3.3.

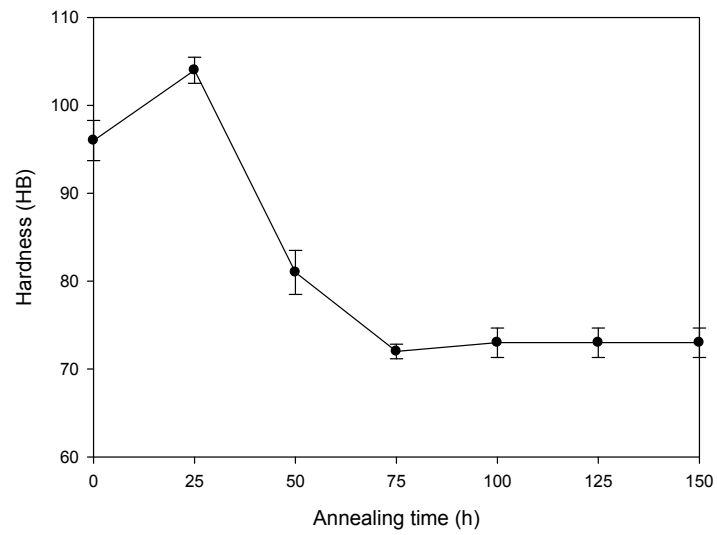


Figure 3.8 Variation of hardness in 5083 Al-alloy samples as a function of the annealing time at 415 °C.



Figure 3.9 Photographs of 5083 Al-alloy specimens in (a) unECAPed (b) ECAPed (c) Annealed (415°C / 144h) + ECAPed conditions.

Table 3.3 Hardness values of the 5083 Al-alloy specimens.

Specimen	Average Hardness (HB)	Specimen	Average Hardness (HB)
As-received	96 ± 3.4	ECAPed	117 ± 2
Annealed (415°C, 144h)	72 ± 1.1	Annealed (415°C, 144h) + ECAPed	116 ± 0

Trial 3: To investigate the deformation of the specimen in the die, square patterns were drawn on the specimen before the process. The square pattern form was not changed but the lines on the upper surface behaved like the crack initiation points and the lines on the lower surface were disappeared due to the high friction. Deformation effect can be seen in lateral surface by changing square pattern into parallelogram (Figure 3.10). Deformation characteristics were seen between the start and finish cracks. Perpendicular lines in the pattern shifted about 58° and became into parallelogram. This shift was in the range of 20 – 25° in the regions close to the lower surface (Figure 3.11). The same study was also done for 6066 Al-alloy and similar results were observed. After the deformation perpendicular lines were shifted about 57°–58° in the pattern seen in Figure 3.12.

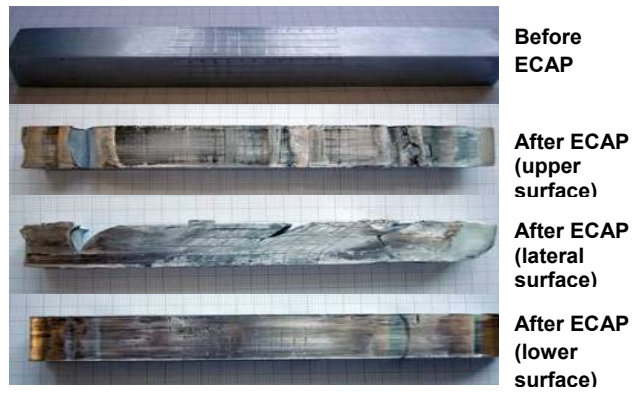


Figure 3.10 Change in square patterns in 5083 Al alloy specimens after ECAP.

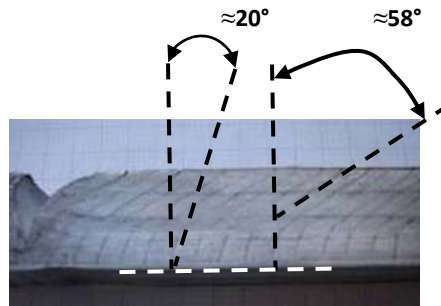


Figure 3.11 Pattern change in the lateral section of 5083 Al alloy specimen after ECAP.

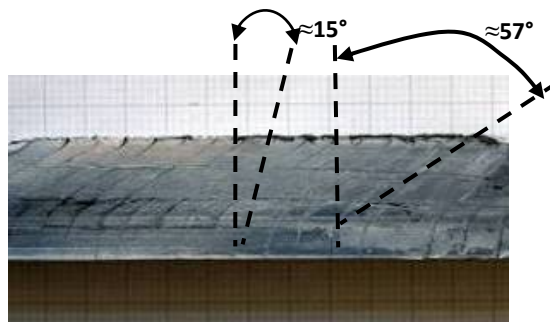


Figure 3.12 Pattern change in the lateral section of 6066 Al alloy specimen after ECAP.

3.2.2. Optimization Studies

The second and final ECAP system was used with horizontal axis hydraulic press. The material of the first ECAP die used with this system having 120° channel angle and square (14x14 mm) cross-section was AISI H13 (hot work tool steel) which was generally used in hot extrusion and press dies. This steel is also suitable for surface treatments, so plasma nitriding was applied to the inside of the die in order to decrease friction by obtaining a smooth surface. The punch of the die having square cross-section was made out of AISI H13 (hot work tool steel) in electro slag remelting (ESR) version.







100 mm long aluminum alloy specimens with 67-73 HB initial hardness were pressed. In the first trial, the specimen was squeezed in the die, and during the second trial, the die was cracked from the diagonal of the die (at the point of the failure, the load of the punch acting on the specimen was 41700 kg. In other words, 212.76 kg load acts per mm² of the specimen). That is why it was decided to construct a die with circular cross-section.

The experiments were continued with a new die having two channels with 120° and circular cross-section (18 mm Φ) presented in Figure 3.13. In other words, the die has two 120° turning points so once the material is pressed through this die; it will be exposed two deformation processes. The material of the die was AISI H13 (hot work tool steel) with hardness value of 56 HRC. In addition, the inside of the die was exposed to plasma nitriding. This die was used again during the optimization of ECAP parameters given in Table 3.4.



Figure 3.13 ECAP die with double 120° channel angle having cross-section with 18 mm Φ .

Table 3.4 ECAP trials of 2024 Al-alloy specimens using the double channel die.

	Remarks	Photo
1	Specimen was tried to pass through the die without back pressure. The leaving specimen was split into parts.	
2	Back pressure about 2.5 – 3 tones was applied to a sample having 60 mm length with the same cross-section. The specimen leaving the die was separated into two with some cracks.	
3	Specimen was emerged into copper before pressing to press the specimen under hydrostatic pressure for inhibiting crack generation since hydrostatic pressure suppresses the crack generation and crack growth. However, it was divided into two with cracks.	
4	The specimens were pre-annealed at 420 °C for 1h, and then ECAPed successfully.	
5	Solutionized sample (495°C / 1h) was passed through the die, but deep cracks were observed.	
6	After first ECAP pass, the sample was machined before the second pass. However, the specimen could not be passed, only a portion of it has turned the first 120° corner.	

3.2.3. Final Trials



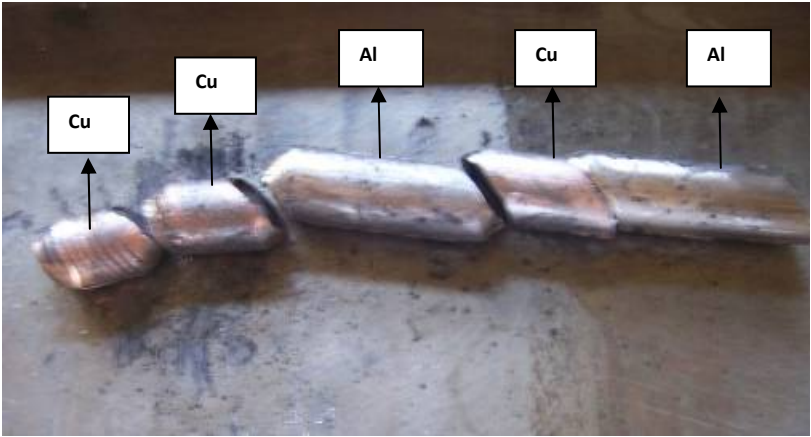
To get rid of die cracks, another die (final die) with the same cross-section was constructed with only one 120° channel. Solutionized 2024 Al-alloy specimens were used in the trials, whose details are given in Table 3.5.

In the light of the preliminary studies, the final design was set and the final specimen condition was determined as solutionizing the 2024 aluminum specimens with a diameter of 18 mm and 100 mm in length at 495 °C for 1 hour (according to ASTM standards) in order not to observe cracks after the process and to apply aging treatment easily after pressing. Solutionizing treatments were done in a muffle furnace. After solutionizing; all of the samples were quenched to 0 °C (ice + water). They were kept in freezer which was maintained at about -18 °C to eliminate natural aging.

All of the ECAP experiments were conducted at room temperature using dies with channel angles of 90° and 120°. It was concluded that required back pressure for an aluminum specimen to pass without any crack is obtained by three copper samples which is equal to the backpressure applied by one aluminum sample plus two copper samples.

Although the maximum pressure applied by the horizontal axis hydraulic press was 400 bar, at the beginning of the feeding the pressure was in the range of 160-180 bar and then the pressure was increased up to 240-260 bar known as working pressure as materials were fed. The load in kilograms applied on the material per mm² was determined by $(\pi \times r^2 \times P / 100)$ where r is the radius of the sample in mm and P is the pressure applied by the punch in bar.

Table 3.5 ECAP trials of 2024 Al-alloy specimens using the single channel die.

	Remarks	Photo
1	Cu rods with 60 mm in length were fed before pressing Al alloy specimen to apply back pressure. When three Cu specimens were pressed for back- pressure, ECAP resulted in no crack.	
2	Cu rods were fed after the specimen. When the specimen was taken out, five Cu rods have remained in the die. So, when the second Al alloy specimen was fed, five Cu rods were ready to apply back-pressure inside the die. However, the back pressure obtained by five Cu rods was excessive so only half of the specimen could turn the corner.	
3	To make this process continuous, it was decided to feed the die with two Cu rods and Al alloy specimen and again two Cu rods and second Al alloy specimen. Unfortunately, second Al could not pass.	
4	Feeding sequence was Cu-Cu-Al-Cu-Al-Cu-Al-Cu-Cu-Al . The bold ones could exit, but the other ones remained in the die. 	

3.3 Experimental Set-up

The final ECAP system was used with horizontal axis hydraulic press given in Figure 3.14. The diameter of the pistons of the system was 125 mm. The final die used with the horizontal axis hydraulic press consisted of two extrusion channels intersecting at an angle of 120° having circular cross-section with 18 mm diameter seen in Figure 3.15 (a). Moreover, the material of the die was AISI H13 (hot work tool steel) die steel with hardness of 56 HR and plasma nitriding was applied to the inside surface of the die. The punch for this circular cross-sectioned die was made out of tungsten carbide seen in Figure 3.15 (b). During pressing, highly purified MoS₂ was used as lubricant in powder form. The powder particles having diameter less than 1 µm were pressed to make tablets with a diameter of 18 mm. These tablets were fed between the specimens during pressing.

3.4. Heat Treatment

The aging treatments, applied both to ECAPed and unECAPed samples, were conducted in the oil bath operating with $\pm 1^\circ\text{C}$ with a system given in Figure 3.16. The medium was silicon oil. Specimens were suspended from the wire attached to the steel container at the top of the bath. After taking out from the bath, the specimens were emerged into toluene and finally cleaned with alcohol.

The aging temperatures and holding durations are given in Table 3.6. UnECAPed aging samples were in the dimensions of 14-14-8 mm whereas ECAPed aging samples were in 18 mm diameter and 8 mm length.

In order to make the grain boundaries apparent for TEM investigations, the samples were annealed at 400 °C for 1 hour. Thermal stability of the microstructure after ECAP was also investigated.

All of the solutionizing and annealing experiments were conducted in a muffle furnace with a maximum operating temperature of 1150 °C. The samples were quenched to 0 °C (ice+ water), and were kept in freezer which was maintained at about -18 °C to avoid natural aging.



Figure 3.14 Horizontal axis hydraulic press.

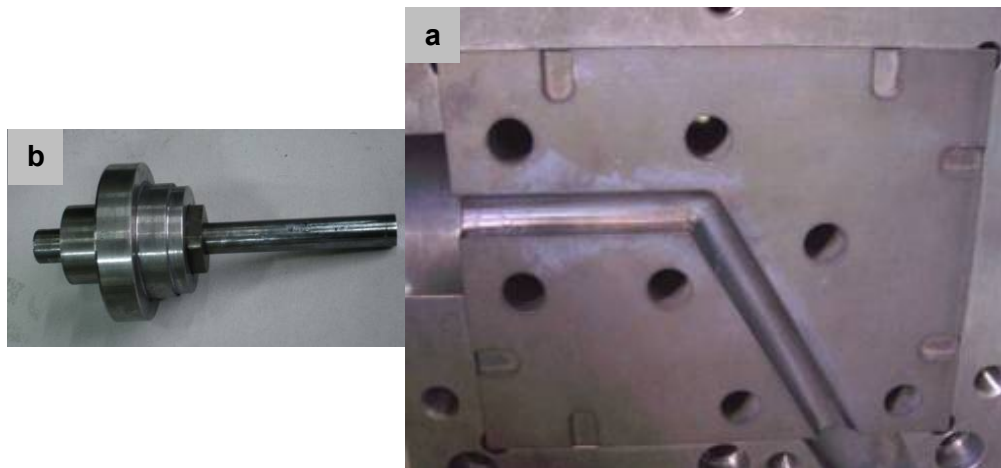


Figure 3.15 (a) ECAP die with 120 ° channel angle having circular (18 mm Φ) cross-section and **(b)** the punch of the die.

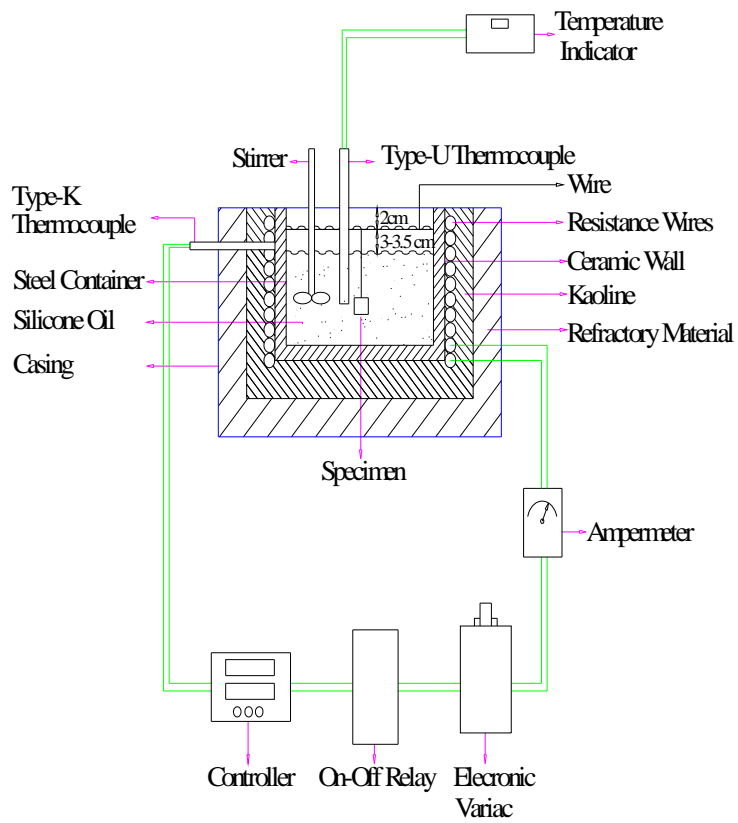


Figure 3.16 Schematic view of the oil bath.

Table 3.6 Aging temperatures and durations.

	T (°C)	time (h)					
		0.5	1	2	4	8	12
undeformed samples	190	0.5	1	2	4	8	12
ECAPed samples	80	30	43	55	65	86	
	100	6	12	24	32	6	12
	190	0.25	0.5	1	2	4	6

3.5 Characterization of Samples

3.5.1 X-Ray Diffraction (XRD)

X-Ray diffractograms were taken by FT (counts) scanning via Rigaku D/Max 2200/PC model X-Ray Diffractometer using Cu K α radiation (at a wavelength of $\lambda=1.54183 \text{ \AA}$). The generator settings were 40 kV and 35 mA. The diffraction data were collected over a 2θ range of both 37.5° to 40° and 97° - 102° from (111) plane, with a step width of 0.02° and a counting time of 5 s per step (FT method). The XRD line-broadening of the ECAPed samples were investigated to determine the subgrain size. Due to the limited size of the sub-grains the peaks broaden. The width, B, measured at an intensity equal to half the maximum intensity termed the full-width at half maximum of FWHM can be related to the cell or sub-grain size, t, with

$$t = (0.9 \lambda) / (B_S \cos\theta_B) \quad (4)$$

where B_S is structural broadening, λ is the wavelength of the radiation used that is 1.54183 \AA and θ_B is the Bragg's angle of the peak in question. B_S is determined with $B_S^2 = B_E^2 - B_R^2$ where B_E is the width measured from ECAPed specimen's peak and includes both of the structural and instrumental broadening whereas B_R is measured from the reference or standard specimen's peak and includes only the instrumental broadening. B_R^2 is subtracted to eliminate the instrumental broadening.

3.5.2 Microstructure

For microstructural characterization, optical microscope (OM), scanning electron microscope (SEM) and transmission electron microscope (TEM) were used to reveal the effect of ECAP process and various heat treatments after ECAP process.

For OM and SEM studies, specimens were cut by Buehler IsoMet® 5000 Linear Precision Saw. The surface of the specimens was ground with 600 and 1200 grit emery papers respectively. Solutionized samples were examined after etching by Keller's reagent (2.5ml HNO₃ + 1.5ml HCl + 1.0ml HF + 95ml water). Optical micrographs were taken by using Nikon FDX-35 camera connected to Nikon Optiphot-100 type microscope. Scanning electron microscope studies were carried out using a Jeol 6400 Scanning Electron Microscope equipped with "Northern Tracor" EDS analysis system.

TEM studies are carried out in TUBITAK-MAM. Specimens were cut by Struers Minitom low speed diamond saw. Thin foils were prepared by disc punching 3 mm disks and grinding down to ~150µm. After that electropolishing was performed with an electrolyte of 25% nitric acid + 75% methanol solution at about -33 °C with 15-20V in Struers-Tenupol-5 Double Jet Electropolisher. Gatan 691 Precision Ion Polishing System (PIPS) was also used to prepare some specimens. Before PIPS 3 mm disks were first ground to 60µm and then the center was thinned down to ~5µm with Gatan 656 Dimple Grinder. Specimens were ion polished first at 5kV and than after transparent area is achieved at final step at 3kV. Specimens were investigated by JEOL 2100 Transmission Electron Microscope 2100 (LaB₆ filament) operated at 200 kV and equipped with an Oxford EDS system. Images were taken both by Gatan Model 694 Slow Scan CCD Camera digitally and also with camera system by developing negative films especially for diffraction patterns. Selected area aperture size was ~50-100 µm. A JEOL side entry double tilt goniometer was used. Dark Field (DF), Bright Field (BF), Selected Area Electron Diffraction (SAED) and Energy Dispersive Spectrometry (EDS) techniques were used to investigate the microstructure.

3.5.3 Hardness Measurements

Hardness measurements were conducted with Heckert analogue hardness machine with 2.5 mm ball. The loads according to the past of the specimens were given in Table 3.7.

Table 3.7 Loads used in Heckert analogue hardness machine.

	N	kp
Solutionized (495 °C, 1h)	306	31.25
Annealed (420 °C, 3h)	306	31.25
Solutionized (495 °C, 1h) + ECAPed	613	62.5
Solutionized (495 °C, 1h) + ECAPed + aged	613	62.5
Solutionized (495 °C, 1h) + ECAPed + annealed	306	31.25

CHAPTER 4

RESULTS AND DISCUSSION

X-ray results were presented to determine the subgrain sizes after ECAP. The variation of microstructure, subgrain formation, dislocation density increase and tangling with ECAP process; subgrain growth after post annealing was presented via TEM. Hardness values both for aging trials and for different conditions of the alloy were tabulated.

4.1. Results of X-Ray Measurements

The X-ray diffractograms for the peak of (111) plane of 2024 Al-alloy specimens in various processing conditions are given in Figure 4.1. After determining the broadening of the ECAPed specimen's peak (B_E) and that of the reference specimen (B_R) at the annealed condition (Figure 4.2), by using Equation 1 the subgrain (cell) size of the ECAPed specimen was calculated as about 50 nm.

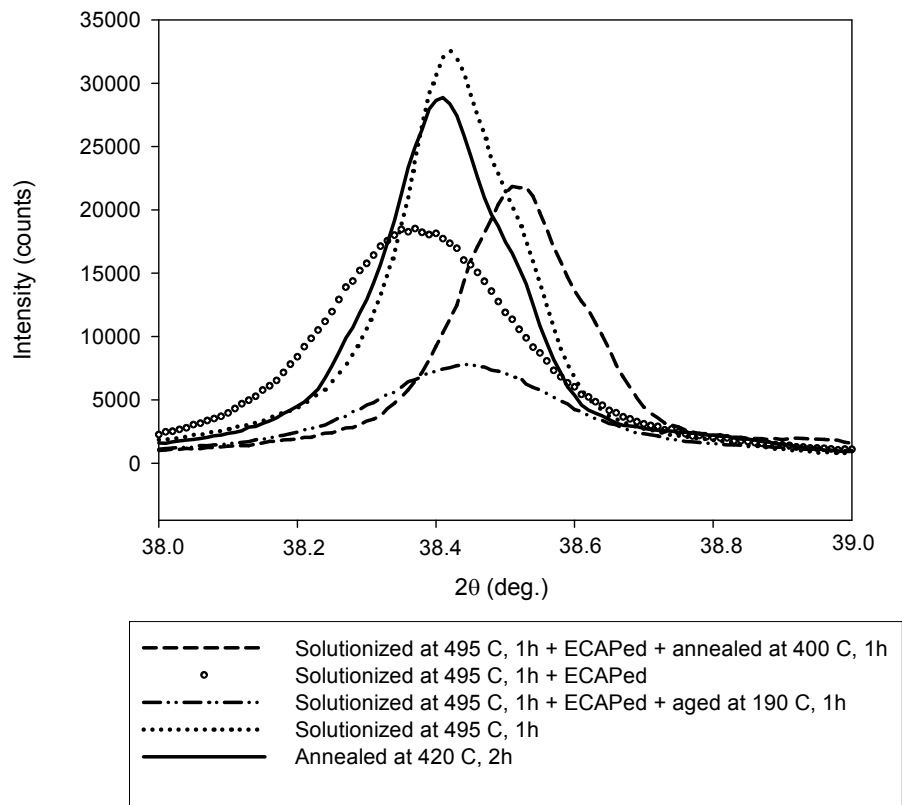


Figure 4.1 X-ray diffraction peaks of (111) plane for specimens in different conditions.

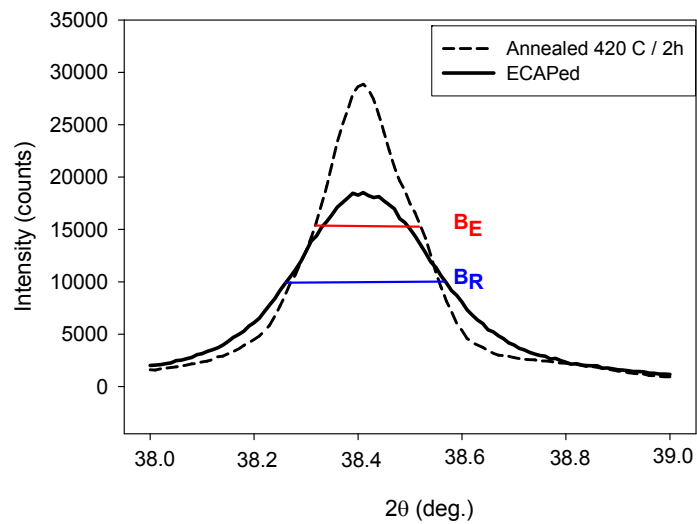


Figure 4.2 X-ray diffraction peaks of (111) plane for annealed and ECAPed specimens.

4.2. Microstructural Investigations

4.2.1. Observations via Optical Microscopy and Scanning Electron Microscopy

Figure 4.3 (a) shows the optical micrograph of the solutionized 2024 Al-alloy showing grain boundaries and inclusions and the grain size distribution is given in Figure 4.3 (b).

SEM images and the chemical compositions of the matrix and inclusion analyzed with EDS were presented in Figure 4.4 and Table 4.1. The EDS analyses are shown in Figure A.1 and Figure A.2 at appendix.

Table 4.1 Chemical compositions of the matrix and inclusion of the solutionized 2024 Al-alloy (EDS analysis).

Element	Matrix		Inclusion	
	Weight Conc. %	Atom Conc. %	Weight Conc. %	Atom Conc. %
Al	94.46	97.40	56.86	74.00
Cu	5.29	2.32	27.91	15.42
Mg	0.25	0.28	-	-
Fe	-	-	8.54	5.37
Mn	-	-	5.15	3.29
Si	-	-	1.54	1.92

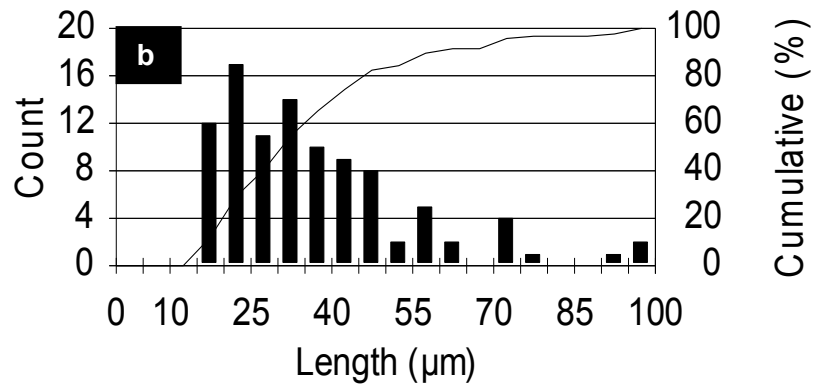
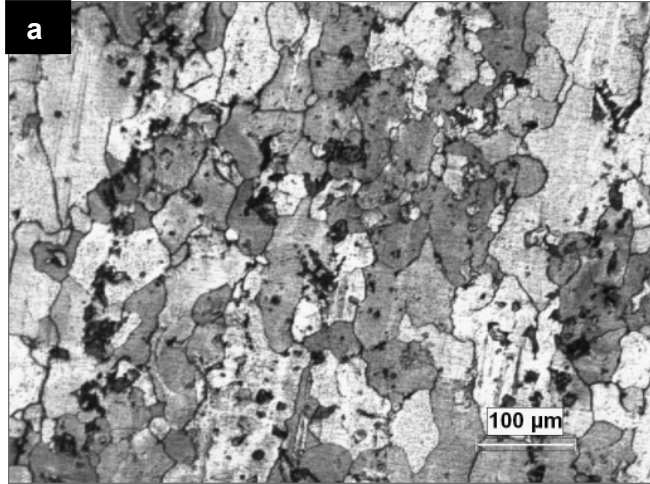


Figure 4.3 Microstructure of 2024 Al-alloy in the solutionized condition: **(a)** Optical micrograph (100X), **(b)** Grain size distribution.

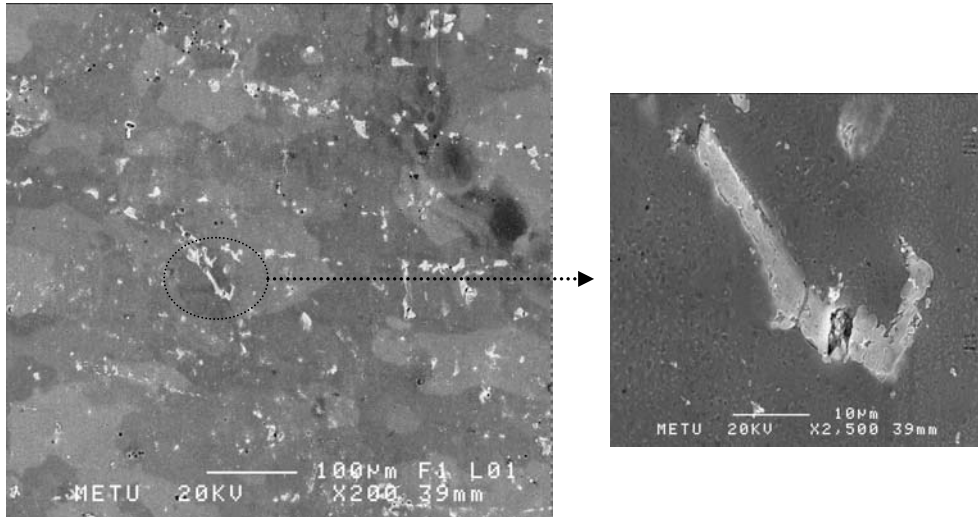


Figure 4.4 SEM micrographs of the solutionized 2024 Al-alloy.

4.2.2. Observations via Transmission Electron Microscopy

Figure 4.5 (a) shows a TEM micrograph showing the microstructure of the as-received Al-alloy having dispersoids in rodlike shape. The chemical composition by EDS analysis of the dispersoid given in Figure 4.5 (b) is presented in Table 4.2. Also the EDS analysis is given in Figure A.3 at appendix. Similar, rodlike shaped dispersoids were clarified as the typical 'T phase' dispersoids observed in 2024 Al-alloys having a composition of $Al_{20}Cu_2Mn_3$, controlling the grain size and acting against recrystallization [11]. As seen in Figure 4.5, dislocations are seen as dark lines due to the cold working without development of well defined (sub) grain boundaries.

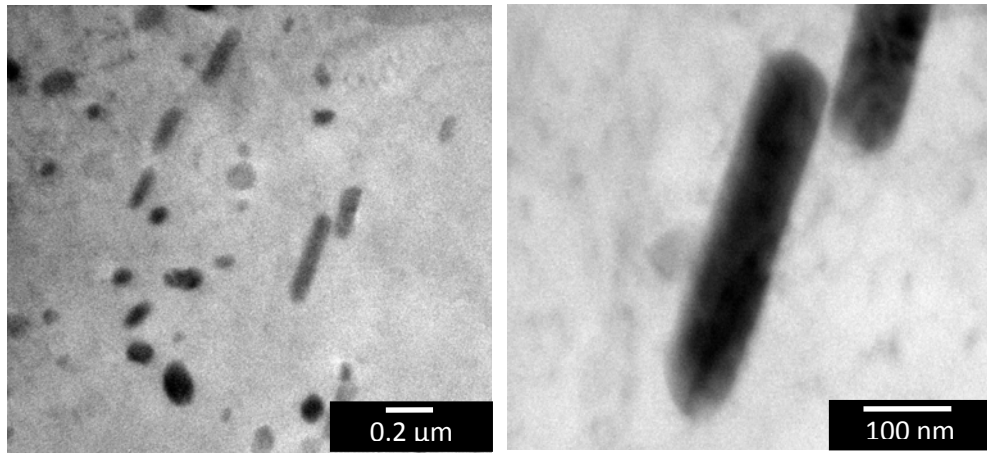


Figure 4.5 a. TEM micrograph of 2024 Al-alloy specimen in as-received condition
b. Rodlike shaped dispersoid.

Table 4.2 Chemical composition of T-phase dispersoid by EDS analysis.

Element	Weight Conc. %	Atom Conc. %
Al	86.81	93.15
Cu	4.70	2.48
Mg	0.69	0.82
Mn	7.79	3.55

Figure 4.6 is a TEM micrograph showing the microstructure of the undeformed 2024 Al-alloy after solid solution treatment having T-phase dispersoids. Figure 4.7 shows the TEM micrographs in bright field and dark field conditions, and corresponding selected area diffraction (SAED) pattern showing the microstructure of ECAPed 2024 Al-alloy. There are some features of sizes similar to subgrain sizes determined by X-ray analysis seen as white areas in Figure 4.7 (b). Very high dislocation density was introduced that is why the individual dislocations cannot be distinguished in the figure

since strain fields fit snugly into each other so the grain boundaries cannot be defined easily. Figure 4.7 (c) shows near-ring pattern, indicating that there are grains with different orientations. Many different orientations are present in the selected area, lead to superpositions of multiple spots which form a series of arcs or a ring pattern. Diffracted patterns are slightly rotated spot patterns and the spots are very close to each other showing that the orientation difference is less compared to Figure 4.7 (c).

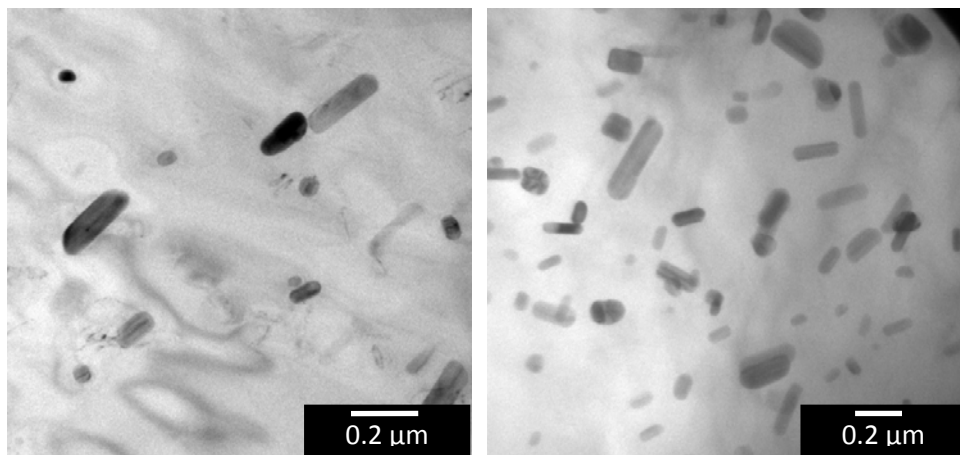


Figure 4.6 TEM micrographs of 2024 Al-alloy in the solutionized condition.

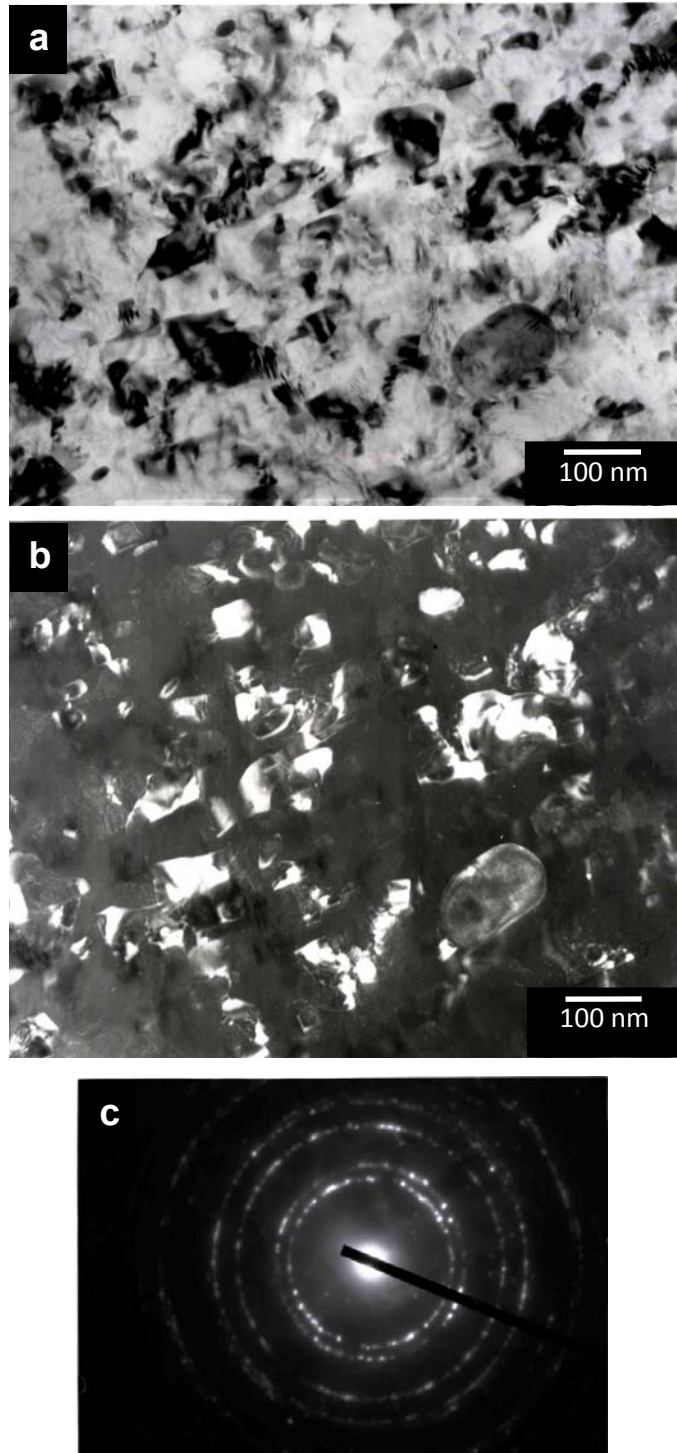


Figure 4.7 TEM images of ECAPed 2024 Al-alloy
a. Bright field **b.** dark field TEM image **c.** SAED patterns.

Dislocations can be seen in Figure 4.8 (a) as dark regions. Although there are bright regions in the figure, dislocations continue but they cannot be detected because of bend contour. This is because the diffraction conditions can be satisfied in somewhere of the specimen seen as dark whereas cannot be satisfied at some regions seen as white due to the bends occurred during the TEM specimen preparation or holding and carrying the specimen. This result is achieved because a sharp transition is not seen in the micrograph from black regions to white areas. Appearance of dislocations as very thin-dark lines between the dark and white regions is a sign of the continuity of dislocations. In Figure 4.8 (b), dislocations are seen to be tangled around a T-phase dispersoid. Moreover, dark and bright areas are interpreted to be dislocation bands and grains without dislocations respectively different than Figure 4.8 (a), because sharp transition is seen from dark to bright regions. Figure 4.8 (c) shows high density of dislocations accumulated around the T-phase dispersoids which is an evidence of inhomogeneous deformation. The advantage of including the T-phase particles in the microstructure which is the ability of acting as obstacles against dislocations is emphasized in literature. In all of the images grain boundaries could not be distinguished due to the superimposed strain fields of high dislocation density. In highly dislocated structures as in this case, the grain size has a minor effect in impeding the motion of the dislocation beside neighboring dislocations.

TEM micrographs of ECAPed and post-annealed (400 °C / 1 h) specimens were given in Figures 4.9 (a,b,c,d) showing the subgrains clearly that are the evidence of recovery. The recovered structure includes dislocation structure inside the subgrains. Average subgrain sizes are determined via Clemex analysis seen in Figures 4.9 (e). The subgrain size of the ECAPed specimen is determined approximately 0.05 μm from X-ray analysis whereas the average subgrain size of the annealed specimen is approximately 0.4 μm . It is the evidence of subgrain growth which is observed during recovery and at the beginning of the recrystallization. This means that, recovery occurs during annealing treatment but the process of recrystallization is not completed. This stems from the insufficient time for complete recrystallization because severely deformed commercial alloys usually can be recrystallized by heating for several hours at 340 to 410°C.

Age hardening treatment was applied both to the unECAPed and ECAPed specimens. Figures 4.10 and 4.11 show the bright field and dark field TEM images of the age hardened specimen at 190 °C for 12 h. The micrographs are constituent with the TEM images shown in Figure 2.4 from literature. Thus, these precipitates are thought to be S' and S'' (Al_2CuMg) precipitates.

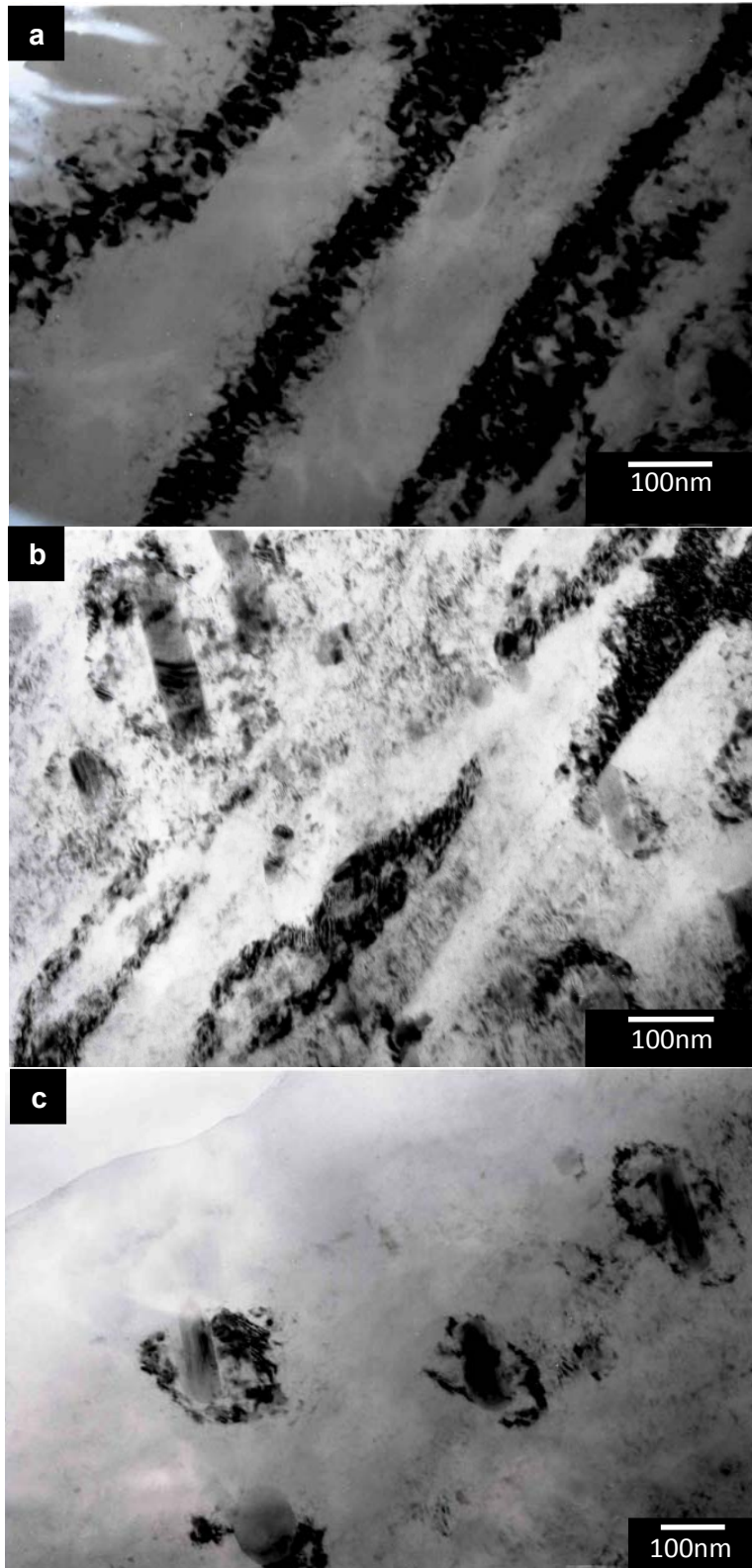


Figure 4.8 TEM micrographs showing dislocation structure of ECAPed 2024 Al-alloy.

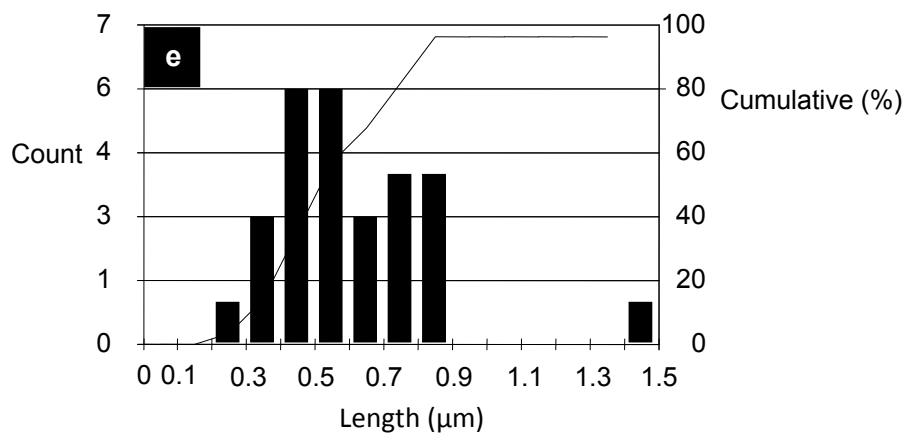
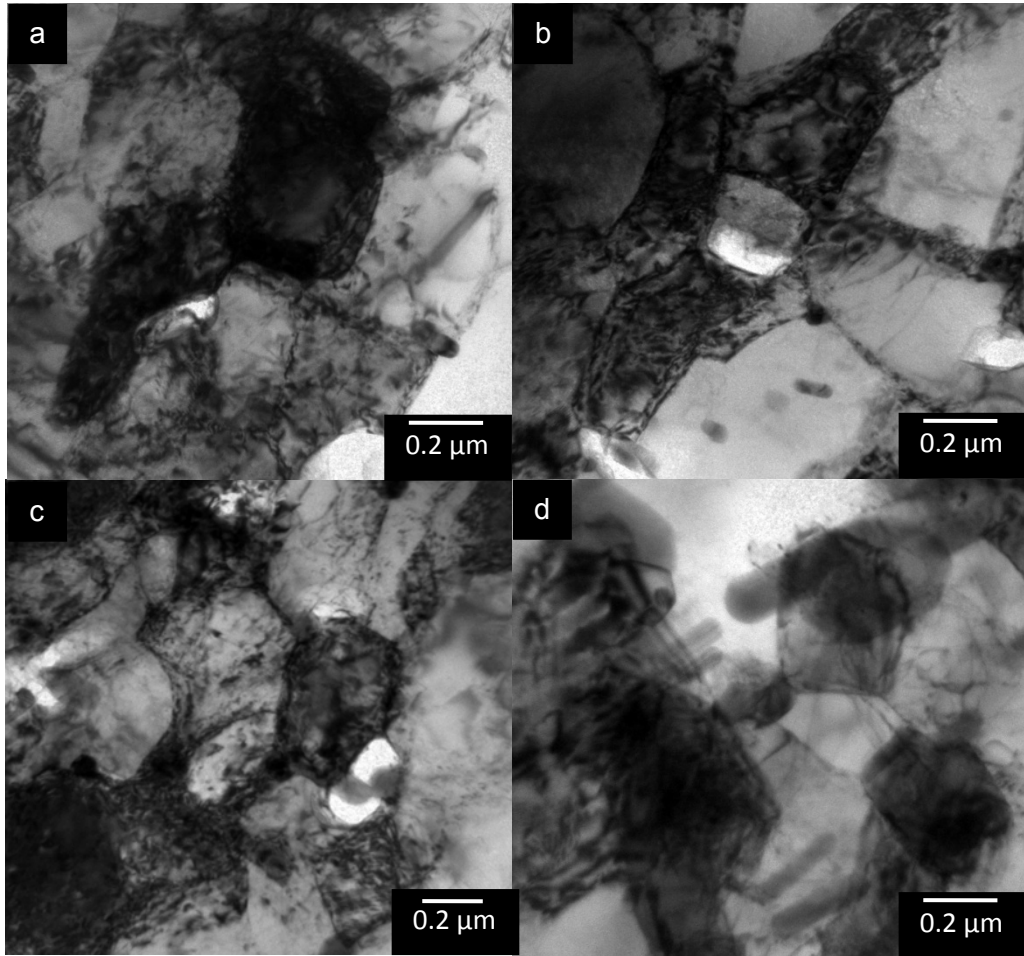


Figure 4.9 a-d. TEM micrographs and **e.** grain size distribution of post-ECAP annealed specimen.

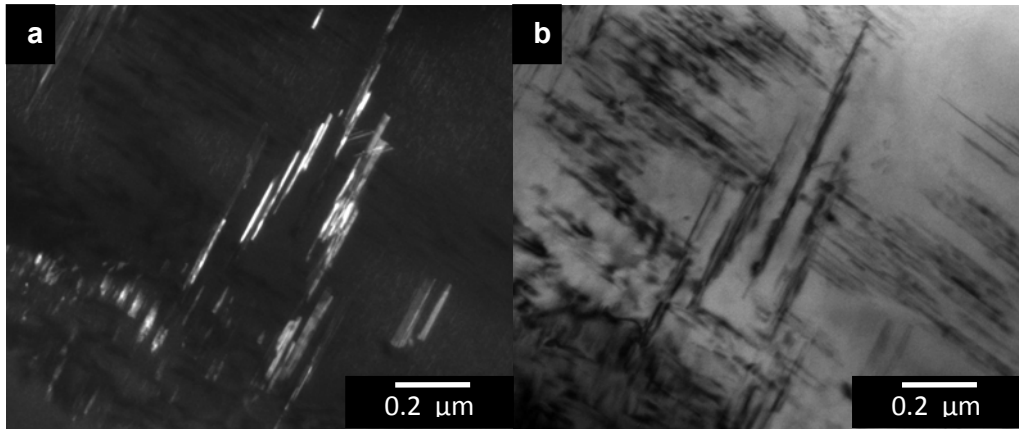


Figure 4.10 **a.** Dark field image **b.** Bright field image of the unECAPed and aged (190°C / 12 h) specimen 1.

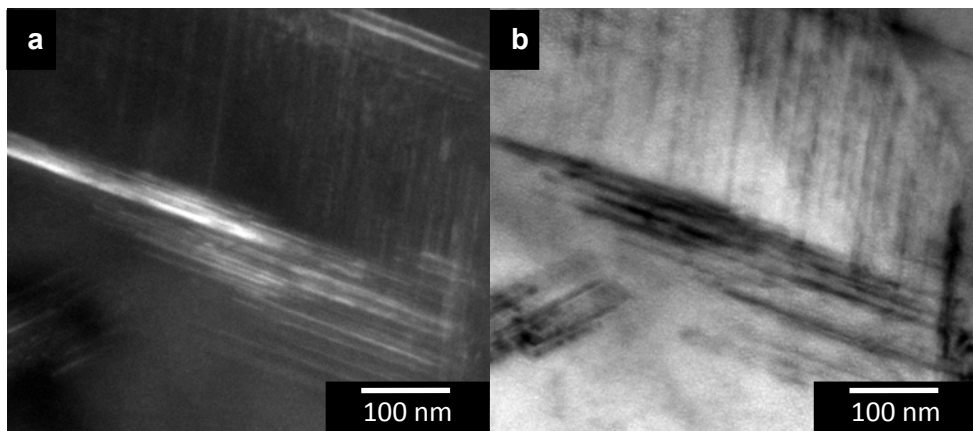


Figure 4.11 **a.** Dark field image **b.** Bright field image of the unECAPed and aged (190°C / 12 h) specimen 2.

The TEM micrograph of the ECAPed plus age hardened (190 °C / 2 h) specimen given in Figure 4.12 shows the precipitates.

Moreover, the EDS analysis result of the age hardened specimen at 190 °C for 12 h is given in Table 4.3 and the EDS analyses are shown in Figure A.5 at appendix. As it can be seen from the table; Al, Cu and Mg elements present in the precipitates of aged specimen that is convenient with the assumption of precipitates are Al₂CuMg. Because the atomic concentrations of Cu and Mg are close to each other and are higher than that of Al. The excess amount of Al may come from the matrix.

The results of X-ray mapping analysis of the age hardened (190 °C / 12 h) specimen given in Figure 4.13 are also shown in Figure B.1 at appendix. It is observed that Al, Si and Mg elements are randomly distributed in the matrix but Mn is seen only in the dispersoids whereas Cu is both distributed in matrix and accumulated in the dispersoids. It is logical since the composition of the dispersoid is Al₂₀Cu₂Mn₃.

Table 4.3 Chemical composition of the precipitates in aged 2024 Al-alloy (EDS analysis).

Element	Weight Conc. %	Atom Conc. %
Al	86.47	91.55
Cu	10.27	4.62
Mg	3.26	3.83

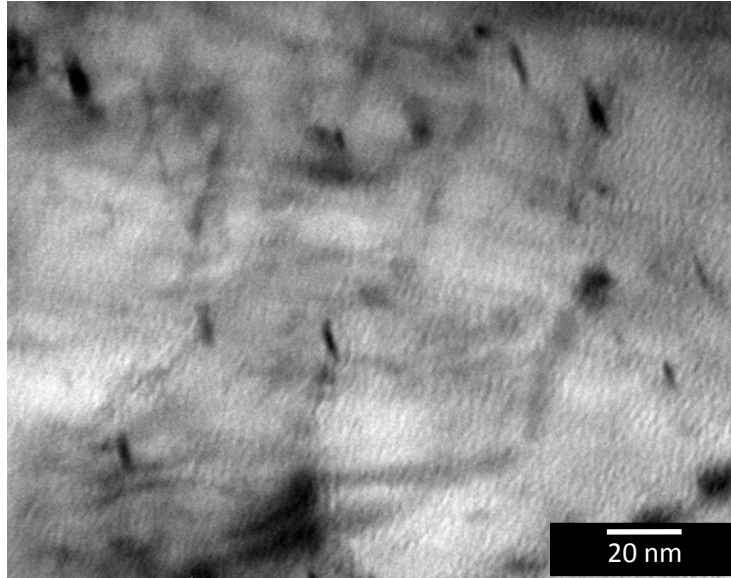


Figure 4.12 TEM micrograph of the ECAPed and age hardened (190 °C / 2 h) specimen.

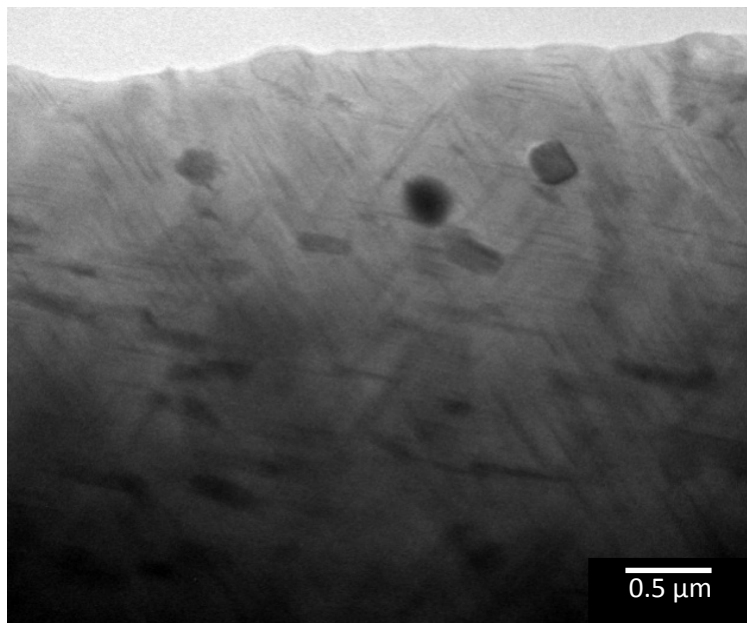


Figure 4.13 TEM micrograph of the aged (190 °C / 12 h) specimen.

4.3. Results of Hardness Measurements

The Brinell hardness values of the specimens in various processing conditions are given in Table 4.4. After 1 pass ECAP, there is a remarkable increase in hardness of the solutionized specimen from ~82 HB to ~160 HB. It is a rule of thumb that the formation of ultra-fine grain structure by ECAP is effective in strengthening due to Hall-Petch relation. Furthermore, the increase in the hardness can be attributed to the high stacking fault energy of aluminum and high density of dislocations. Due to the ability of dislocations to cross-slip, they may be condensed into tangles and formed dislocation-free subgrains.

Table 4.4 Hardness values of 2024 Al alloy specimen in different conditions.

	Hardness (HB)
As-received	141 ± 6
Solutionized (495°C / 1h)	82 ± 1
Annealed (420°C / 3h)	64 ± 1
Solutionized + ECAP	160 ± 11
Solutionized + ECAP + annealed (400°C / 1h)	72 ± 1
Solutionized + annealed (400°C / 1h)	69 ± 3
Solutionized + ECAP + peak aged (190°C / 1h)	189 ± 8
Solutionized + peak aged (190°C / 24h)	142 ± 6

As it is mentioned, the solutionized and the solutionized+ECAPed specimens were exposed to age hardening treatment. The most promising results were obtained by investigating the aging performance of the specimens. After aging process hardness values of both of the specimens increased up to a peak value and then decreased with time due to overaging as usual. There was retardation in the peak value in the

ECAPed specimens as temperature decreases. Moreover, the remarkable effect of ECAP process on age hardening behavior of the alloy as a function of time was presented in Figure 4.14. A peak hardness of 141 HB could be attained after 24 h of aging for the solutionized case whereas a peak hardness value of 198 HB was reached in considerably shorter time (~ 1 h) after ECAP by applying the same aging process. These results show the accelerating effect of ECAP on age hardening process. Besides, the creation of dislocations in the matrix during ECAP was most likely to serve as nucleation sites for precipitates like dispersoids leading to an increase in heterogeneous nucleation. Therefore, precipitation rate is increased leading to a decrease in precipitation temperature or time needed for obtaining peak hardness at a given temperature. Moreover, as the aging temperature increases the profile shifts to the shorter times.

Softening is expected in metals with high SFE like Al during recovery anneal because hardness is related with the concentration and distribution of dislocations. The hardness value decreased to 72 HB with post-ECAP annealing treatment due to the rearrangement of dislocations forming subgrains.

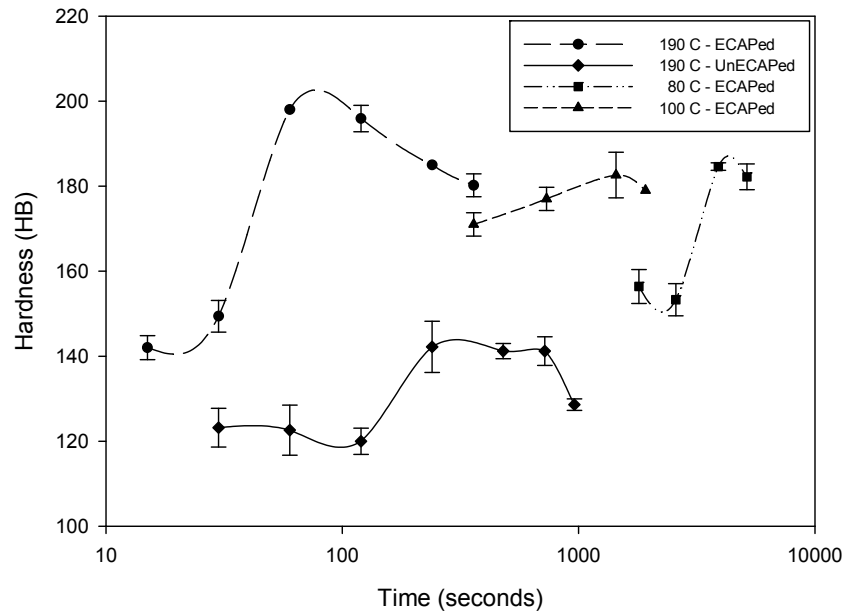


Figure 4.14 Hardness versus aging time (in seconds) graph of ECAPed and unECAPed specimens.

CHAPTER 5

CONCLUSION

The combined effects of equal channel angular pressing (ECAP) and subsequent heat treatments, i.e. post-aging and post-annealing, on the microstructure and hardness of the 2024 aluminum alloy were investigated. An ECAP die with 120° channel angle was used for severe plastic deformation of the samples at room temperature.

TEM investigations of the deformed (one-pass ECAP) and deformed-heat treated samples showed: extremely high dislocation density and dislocation tangles around dispersoids after ECAP; subgrain growth after ECAP+annealing; and precipitates and dislocations after ECAP+aging. The sizes of the subgrains were determined via X-ray diffraction method.

The following conclusions were drawn from the results:

- Ultra-fine grain size can be obtained by ECAP.
- Significant increase in the hardness (from ~82 HB to ~160 HB) was obtained after ECAP. It can be attributed to the increase in dislocation density and ultra-fine grain size.
- Further increase in the hardness up to 198 HB by subsequent aging treatment is due to the formation of dispersed S' and S precipitates. As the aging temperature of the ECAPed samples increases, higher peak values were obtained at shorter times comparing to those obtained by sole application of aging. This accelerating effect of ECAP on age hardening is attributed to the action of dislocations as nucleation sites for the precipitates.
- A combined process of ECAP and subsequent aging is a promising manufacturing route to improve the strength of the 2024 Al-alloy. However, it is necessary to repeat the similar investigations after multi-pass ECAP, and also to perform some other mechanical tests for decision on the applicability of this route in industrial applications.

REFERENCES

- [1] J.R. Davis, ASM Speciality Handbook - Aluminum and Aluminum Alloys.
- [2] G.E. Dieter, Mechanical Metallurgy, 2001.
- [3] A. Kelly, Strong Solids, 1973.
- [4] R.Z. Valiev, R.K. Islamgaliev, and I.V. Alexandrov, Bulk nanostructured materials from severe plastic deformation. *Progress in Materials Science* 45 (2000) 103-189.
- [5] P.J. Apps, J.R. Bowen, and P.B. Prangnell, The Effect of Second-Phase Particles on the Severe Deformation of Aluminum Alloys during Equal Channel Angular Extrusion. in: M. Zehetbauer, and R.Z. Vailev, (Eds.), *Nanomaterials by Severe Plastic Deformation - NANOSPD2*, Vienna, Austria, 2002, pp. 138-144.
- [6] P.J. Apps, and P.B. Prangnell, Grain Refinement Mechanisms Operating During Severe Deformation of Aluminum Alloys Containing Second-Phase Particles. in: Y.T. Zhu, T.G. Langdon, R.Z. Vailev, S.L. Semiatin, D.H. Shin, and T.C. Lowe, (Eds.), *Ultrafine Grained Materials III*, North Carolina, U.S.A., 2004, pp. 131-136.
- [7] S.C. Wang, and M.J. Starink, Precipitates and intermetallic phases in precipitation hardening Al-Cu-Mg-(Li) based alloys. *Int Mater Rev.* 50 (2005) 193-215.
- [8] A. Charai, T. Walther, C. Alfonso, A.M. Zahra, and C.Y. Zahra, Coexistence of clusters, GPB zones, S^{''}-, S[']- and S-phases in an Al-0.9% Cu-1.4% Mg alloy. *Acta Materialia* 48 (2000) 2751-2764.
- [9] S.C. Wang, M.J. Starink, and N. Gao, Precipitation hardening in Al-Cu-Mg alloys revisited. *Scripta Materialia* 54 (2006) 287-291.
- [10] L.B. Ber, Accelerated artificial ageing regimes of commercial aluminum alloys. I. Al-Cu-Mg alloys. *Materials Science and Engineering A* 280 (2000) 83-90.

- [11] S. Cheng, Y.H. Zhao, Y.T. Zhu, and E. Ma, Optimizing the strength and ductility of fine structured 2024 Al alloy by nano-precipitation. *Acta Materialia* 55 (2007) 5822-5832.
- [12] R.Z. Valiev, and R.Z. Langdon, Principles of equal-channel angular pressing as a processing tool for grain refinement. *Progress in Materials Science* (2006) 881-981.
- [13] S. Firstov, M. Brodnikovskiy, M. Danylenko, and Y. Podrezov, Nanocrystalline structure formation under severe plastic deformation and its influences on mechanical properties. *Rev. Adv. Mater. Sci.* 4 (2003) 155-162.
- [14] H. Mughrabi, H.W. Höppel, M. Kautz, and R.Z. Valiev, Annealing treatments to enhance thermal and mechanical stability of ultrafine-grained metals by severe plastic deformation. *Z. Metallkunde* 94 (2003) 1079-1083.
- [15] J.W. Park, J.W. Kim, and Y.H. Chung, Grain refinement of steel plate by continuous equal-channel angular process. *Scripta Materialia* 51 (2004) 181-184.
- [16] R.Z. Valiev, A.V. Korznikov, and R.R. Mulyukov, Structure and properties of ultrafine-grained materials produced by severe plastic deformation. *Materials Science and Engineering A* 168 (1993) 141-148.
- [17] R.Z. Vailev, N.A. Krasilnikov, and N.K. Tsenev, Plastic Deformation of Alloys with Submicro-Grained Structure. *Materials Science and Engineering A* 137 (1991) 35-40.
- [18] R.Z. Valiev, Y.V. Ivanisenko, E.F. Rauch, and B. Baudalet, Structure and deformation behaviour of Armco iron subjected to severe plastic deformation. *Acta Materialia* 44 (1996) 4705-4712.
- [19] M. Furukawa, Z. Horita, M. Nemoto, and T.G. Langdon, The use of severe plastic deformation for microstructural control. *Materials Science and Engineering a-Structural Materials Properties Microstructure and Processing* 324 (2002) 82-89.

- [20] A.A. Mazilkin, B.B. Straumal, E. Rabkin, B. Baretzky, S. Enders, S.G. Protasova, O.A. Kogtenkova, and R.Z. Valiev, Softening of nanostructured Al-Zn and Al-Mg alloys after severe plastic deformation. *Acta Materialia* 54 (2006) 3933-3939.
- [21] A.V. Sergueeva, V.V. Stolyarov, R.Z. Valiev, and A.K. Mukherjeeb, Enhanced superplasticity in a Ti-6Al-4V alloy processed by severe plastic deformation. *Scripta Materialia* 43 (2000) 819-824.
- [22] O.V. Rybal'chenko, S.V. Dobatkin, L.M. Kaputkina, G.I. Raab, and N.A. Krasilnikov, Strength of ultrafine-grained corrosion-resistant steels after severe plastic deformation. *Materials Science and Engineering a-Structural Materials Properties Microstructure and Processing* 387-89 (2004) 244-248.
- [23] G. Sakai, Z. Horita, and T.G. Langdon, Grain refinement and superplasticity in an aluminum alloy processed by high-pressure torsion. *Materials Science and Engineering a-Structural Materials Properties Microstructure and Processing* 393 (2005) 344-351.
- [24] Y. Iwahashi, J. Wang, Z. Horita, M. Nemoto, and T.G. Langdon, Principles of equal-channel angular pressing for the processing of ultra-fine grained materials. *Scripta Materialia* 35 (1996) 143-146.
- [25] V.M. Segal, Materials Processing By Simple Shear. *Materials Science and Engineering a-Structural Materials Properties Microstructure and Processing* 197 (1995) 157-164.
- [26] Y. Iwahashi, Z. Horita, M. Nemoto, and T.G. Langdon, The process of grain refinement in equal-channel angular pressing. *Acta Materialia* 46 (1998) 3317-3331.
- [27] Y. Iwahashi, Z. Horita, M. Nemoto, and T.G. Langdon, An investigation of microstructural evolution during equal-channel angular pressing. *Acta Materialia* 45 (1997) 4733-4741.

- [28] C. Xu, M. Furukawa, Z. Horita, and T.G. Langdon, Severe plastic deformation as a processing tool for developing superplastic metals. *Journal of Alloys and Compounds* 378 (2004) 27-34.
- [29] J. Gubicza, N.Q. Chinh, T. Csanádi, T.G. Langdon, and T. Ungár, Microstructure and strength of severely deformed fcc metals. *Materials Science and Engineering: A* 462 (2007) 86-90.
- [30] Y.H. Zhao, X.Z. Liao, Z. Jin, R.Z. Valiev, and Y.T. Zhu, Microstructures and mechanical properties of ultrafine grained 7075 Al alloy processed by ECAP and their evolutions during annealing. *Acta Materialia* 52 (2004) 4589-4599.
- [31] A.V. Nagasekhar, and Y. Tick-Hon, Optimal tool angles for equal channel angular extrusion of strain hardening materials by finite element analysis. *Computational Materials Science* 30 (2004) 489-495.
- [32] J. Gubicza, N.Q. Chinh, G. Krallics, I. Schiller, and T. Ungar, Microstructure of ultrafine-grained fcc metals produced by severe plastic deformation. *Current Applied Physics* 6 (2006) 194-199.
- [33] C.W. Su, B.W. Chua, L. Lu, and M.O. Lai, Properties of severe plastically deformed Mg alloys. *Materials Science and Engineering a-Structural Materials Properties Microstructure and Processing* 402 (2005) 163-169.
- [34] A. Mishra, B.K. Kad, F. Gregori, and M.A. Meyers, Microstructural evolution in copper subjected to severe plastic deformation: Experiments and analysis. *Acta Materialia* 55 (2007) 13-28.
- [35] J.A. del Valle, F. Carreno, and O.A. Ruano, Influence of texture and grain size on work hardening and ductility in magnesium-based alloys processed by ECAP and rolling. *Acta Materialia* 54 (2006) 4247-4259.
- [36] E. Cerri, and P. Leo, Influence of severe plastic deformation on aging of Al-Mg-Si alloys. *Materials Science and Engineering a-Structural Materials Properties Microstructure and Processing* 410 (2005) 226-229.

- [37] Y. Fukuda, K. Oh-ishi, M. Furukawa, Z. Horita, and T.G. Langdon, Influence of crystal orientation on ECAP of aluminum single crystals. *Materials Science and Engineering a-Structural Materials Properties Microstructure and Processing* 420 (2006) 79-86.
- [38] J. Mao, S.B. Kang, and J.O. Park, Grain refinement, thermal stability and tensile properties of 2024 aluminum alloy after equal-channel angular pressing. *Journal of Materials Processing Technology* 159 (2005) 314-320.
- [39] M. Sus-Ryszkowska, T. Wejrzanowski, Z. Pakiela, and K.J. Kurzydowski, Microstructure of ECAP severely deformed iron and its mechanical properties. *Materials Science and Engineering a-Structural Materials Properties Microstructure and Processing* 369 (2004) 151-156.
- [40] R.B. Figueiredo, and T.G. Langdon, The development of superplastic ductilities and microstructural homogeneity in a magnesium ZK60 alloy processed by ECAP. *Materials Science and Engineering a-Structural Materials Properties Microstructure and Processing* 430 (2006) 151-156.
- [41] G.J. Raab, R.Z. Valiev, T.C. Lowe, and Y.T. Zhu, Continuous processing of ultrafine grained Al by ECAP-Conform. *Materials Science and Engineering a-Structural Materials Properties Microstructure and Processing* 382 (2004) 30-34.
- [42] I.V. Alexandrov, M.V. Zhilina, A.V. Scherbakov, and J.T. Bonarski, Multiscale investigations of severe plastic deformation. *Materials Science and Engineering a-Structural Materials Properties Microstructure and Processing* 410 (2005) 332-336.
- [43] J. Gubicza, N.Q. Chinh, T. Csanadi, T.G. Langdon, and T. Ungar, Microstructure and strength of severely deformed fcc metals. *Materials Science and Engineering a-Structural Materials Properties Microstructure and Processing* 462 (2007) 86-90.
- [44] R.Z. Valiev, A.V. Sergueeva, and A.K. Mukherjee, The effect of annealing on tensile deformation behavior of nanostructured SPD titanium. *Scripta Materialia* 49 (2003) 669-674.

- [45] R.S. Mishra, V.V. Stolyarov, C. Echer, R.Z. Valiev, and A.K. Mukherjee, Mechanical behavior and superplasticity of a severe plastic deformation processed nanocrystalline Ti-6Al-4V alloy. *Materials Science and Engineering a-Structural Materials Properties Microstructure and Processing* 298 (2001) 44-50.
- [46] S.Y. Li, A.A. Gazder, I.J. Beyerlein, C.H.J. Davies, and E.V. Pereloma, Microstructure and texture evolution during equal channel angular extrusion of interstitial-free steel: Effects of die angle and processing route. *Acta Materialia* 55 (2007) 1017-1032.
- [47] K.-T. Park, Y.-S. Kim, J.G. Lee, and D.H. Shin, Thermal stability and mechanical properties of ultrafine grained low carbon steel. *Materials Science and Engineering A* 293 (2000) 165-172.
- [48] C. Pithan, T. Hashimoto, M. Kawazoe, J. Nagahora, and K. Higashi, Microstructure and texture evolution in ECAE processed A5056. *Materials Science and Engineering a-Structural Materials Properties Microstructure and Processing* 280 (2000) 62-68.
- [49] K. Nakashima, Z. Horita, M. Nemoto, and T.G. Langdon, Development of a multi-pass facility for equal-channel angular pressing to high total strains. *Materials Science and Engineering a-Structural Materials Properties Microstructure and Processing* 281 (2000) 82-87.
- [50] K. Matsuki, T. Aida, T. Takeuchi, J. Kusui, and K. Yokoe, Microstructural characteristics and superplastic-like behavior in aluminum powder alloy consolidated by equal-channel angular pressing. *Acta Materialia* 48 (2000) 2625-2632.
- [51] M. Furukawa, Y. Iwahashi, Z. Horita, M. Nemoto, and T.G. Langdon, The shearing characteristics associated with equal-channel angular pressing. *Materials Science and Engineering a-Structural Materials Properties Microstructure and Processing* 257 (1998) 328-332.

- [52] S. Lee, M. Furukawa, Z. Horita, and T.G. Langdon, Developing a superplastic forming capability in a commercial aluminum alloy without scandium or zirconium additions. *Materials Science and Engineering a-Structural Materials Properties Microstructure and Processing* 342 (2003) 294-301.
- [53] B.S. Moon, H.S. Kim, and S.I. Hong, Plastic flow and deformation homogeneity of 6061 Al during equal channel angular pressing. *Scripta Materialia* 46 (2002) 131-136.
- [54] S.C. Baik, Y. Estrin, H.S. Kim, and R.J. Hellmig, Dislocation density-based modeling of deformation behavior of aluminium under equal channel angular pressing. *Materials Science and Engineering a-Structural Materials Properties Microstructure and Processing* 351 (2003) 86-97.
- [55] S.J. Oh, and S.B. Kang, Analysis of the billet deformation during equal channel angular pressing. *Materials Science and Engineering a-Structural Materials Properties Microstructure and Processing* 343 (2003) 107-115.
- [56] K. Nakashima, Z. Horita, M. Nemoto, and T.G. Langdon, Influence of channel angle on the development of ultrafine grains in equal-channel angular pressing. *Acta Materialia* 46 (1998) 1589-1599.
- [57] W. Wei, G. Chen, and J. Wang, Influence of Outer Arc Angle on Mechanical Properties of Pure Copper in Equal Channel Angular Pressing. in: Y.T. Zhu, T.G. Langdon, R.Z. Valiev, S.L. Semiatin, D.H. Shin, and T.C. Lowe, (Eds.), *Ultrafine Grained Materials III*, North Carolina, U.S.A., 2004, pp. 155-160.
- [58] A. Yamashita, D. Yamaguchi, Z. Horita, and T.G. Langdon, Influence of pressing temperature on microstructural development in equal-channel angular pressing. *Materials Science and Engineering a-Structural Materials Properties Microstructure and Processing* 287 (2000) 100-106.
- [59] I. Mazurina, T. Sakai, H. Miura, O. Sitdikov, and R. Kaibyshev, Effect of deformation temperature on microstructure evolution in aluminum alloy 2219 during hot ECAP. *Materials Science and Engineering: A* 486 (2008) 662-671.

- [60] B.Q. Han, and T.G. Langdon, Achieving enhanced tensile ductility in an Al-6061 composite processed by severe plastic deformation. *Materials Science and Engineering a-Structural Materials Properties Microstructure and Processing* 410 (2005) 430-434.
- [61] D. Yamaguchi, Z. Horita, M. Nemoto, and T.G. Langdon, Significance of adiabatic heating in equal-channel angular pressing. *Scripta Materialia* 41 (1999) 791-796.
- [62] V.V. Stolyarov, R. Lapovok, I.G. Brodova, and P.F. Thomson, Ultrafine-grained Al-5 wt.% Fe alloy processed by ECAP with backpressure. *Materials Science and Engineering a-Structural Materials Properties Microstructure and Processing* 357 (2003) 159-167.
- [63] S.L. Semiatin, D.P. Delo, and E.B. Shell, The effect of material properties and tooling design on deformation and fracture during equal channel angular extrusion. *Acta Materialia* 48 (2000) 1841-1851.
- [64] H.J. Roven, H. Nesboe, J.C. Werenskiold, and T. Seibert, Mechanical properties of aluminium alloys processed by SPD: Comparison of different alloy systems and possible product areas. *Materials Science and Engineering a-Structural Materials Properties Microstructure and Processing* 410 (2005) 426-429.
- [65] Z. Horita, T. Fujinami, M. Nemoto, and T.G. Langdon, Improvement of mechanical properties for Al alloys using equal-channel angular pressing. *Journal of Materials Processing Technology* 117 (2001) 288-292.
- [66] Y.T. Zhu, and T.G. Langdon, The Fundamentals of Nanostructured Materials Processed by Severe Plastic Deformation. *Journal of the Minerals, Metals and Materials Society* 56 (2004) 58-63.
- [67] G.W. Rowe, *Principles of Industrial Metalworking Processes*, 1977.
- [68] D.A. Porter, and K.E. Easterling, *Phase Transformations in Metals and Alloys*, 1981.

- [69] H.G. Kang, J.P. Lee, M.Y. Huh, and O. Engler, Stability against coarsening in ultra-fine grained aluminum alloy AA 3103 sheet fabricated by continuous confined strip shearing. *Materials Science and Engineering a-Structural Materials Properties Microstructure and Processing* 486 (2008) 470-480.
- [70] W.J. Kim, C.S. Chung, D.S. Ma, S.I. Hong, and H.K. Kim, Optimization of strength and ductility of 2024 Al by equal channel angular pressing (ECAP) and post-ECAP aging. *Scripta Materialia* 49 (2003) 333-338.
- [71] M. Murayama, Z. Horita, and K. Hono, Microstructure of two-phase Al-1.7 at% Cu alloy deformed by equal-channel angular pressing. *Acta Materialia* 49 (2001) 21-29.
- [72] J.K. Kim, H.G. Jeong, S.I. Hong, Y.S. Kim, and W.J. Kim, Effect of aging treatment on heavily deformed microstructure of a 6061 aluminum alloy after equal channel angular pressing. *Scripta Materialia* 45 (2001) 901-907.
- [73] D.R. Fang, Z.F. Zhang, S.D. Wu, C.X. Huang, H. Zhang, N.Q. Zhao, and J.J. Li, Effect of equal channel angular pressing on tensile properties and fracture modes of casting Al-Cu alloys. *Materials Science and Engineering a-Structural Materials Properties Microstructure and Processing* 426 (2006) 305-313.
- [74] L.J. Zheng, H.X. Li, M.F. Hashmi, C.Q. Chen, Y. Zhang, and M.G. Zeng, Evolution of microstructure and strengthening of 7050 Al alloy by ECAP combined with heat-treatment. *Journal of Materials Processing Technology* 171 (2006) 100-107.
- [75] W.J. Kim, and J.Y. Wang, Microstructure of the post-ECAP aging processed 6061 Al alloys. *Materials Science and Engineering A* 464 (2007) 23-27.
- [76] W.J. Kim, J.K. Kim, H.K. Kim, J.W. Park, and Y.H. Jeong, Effect of post equal-channel-angular-pressing aging on the modified 7075 Al alloy containing Sc. *Journal of Alloys and Compounds* 450 (2008) 222-228.
- [77] J.D. Verhoeven, *Fundamentals of physical metallurgy*, 1934.

- [78] L.J. Zheng, C.Q. Chen, T.T. Zhou, P.Y. Liu, and M.G. Zeng, Structure and properties of ultrafine-grained Al-Zn-Mg-Cu and Al-Cu-Mg-Mn alloys fabricated by ECA pressing combined with thermal treatment. *Materials Characterization* 49 (2003) 455-461.
- [79] D.G. Morris, and M.A. Munoz-Morris, Microstructure of severely deformed Al-3Mg and its evolution during annealing. *Acta Materialia* 50 (2002) 4047-4060.
- [80] H. Hasegawa, S. Komura, A. Utsunomiya, Z. Horita, M. Furukawa, M. Nemoto, and T.G. Langdon, Thermal stability of ultrafine-grained aluminum in the presence of Mg and Zr additions. *Materials Science and Engineering A* 265 (1999) 188-196.
- [81] C.Y. Yu, P.L. Sun, P.W. Kao, and C.P. Chang, Evolution of microstructure during annealing of a severely deformed aluminum. *Materials Science and Engineering A* 366 (2004) 310-317.
- [82] M.A. Munoz-Morris, C.G. Oca, G. Gonzalez-Doncel, and D.G. Morris, Microstructural evolution of dilute Al-Mg alloys during processing by equal channel angular pressing and during subsequent annealing. *Materials Science and Engineering a-Structural Materials Properties Microstructure and Processing* 375-77 (2004) 853-856.
- [83] W.Q. Cao, A. Godfrey, W. Liu, and Q. Liu, Annealing behavior of aluminium deformed by equal channel angular pressing. *Materials Letters* 57 (2003) 3767-3774.
- [84] W.Q. Cao, A. Godfrey, W. Liu, and Q. Liu, EBSD study of the annealing behavior of aluminum deformed by equal channel angular processing. *Materials Science and Engineering a-Structural Materials Properties Microstructure and Processing* 360 (2003) 420-425.
- [85] M. Furukawa, Y. Iwahashi, Z. Horita, M. Nemoto, N.K. Tsenev, R.Z. Valiev, and T.G. Langdon, Structural evolution and the Hall-Petch relationship in an Al-Mg-Li-Zr alloy with ultra-fine grain size. *Acta Materialia* 45 (1997) 4751-4757.

APPENDIX A

EDS ANALYSIS

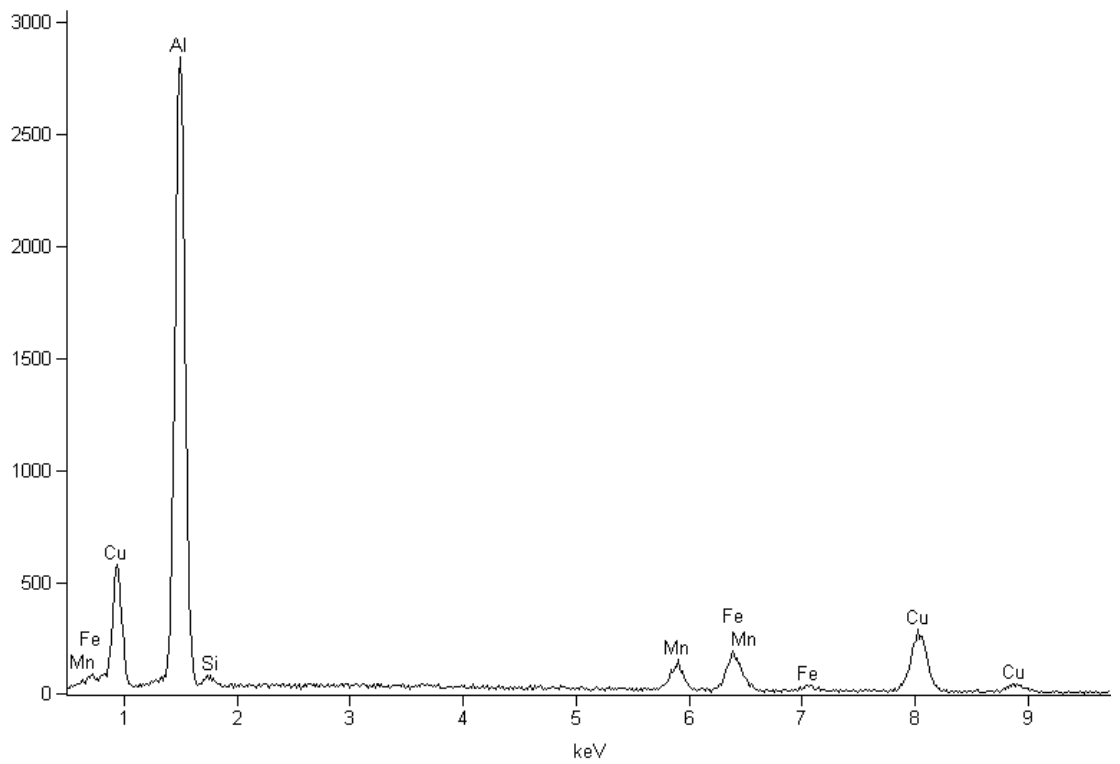


Figure A.1 EDS analysis of inclusions in the solutionized specimen.

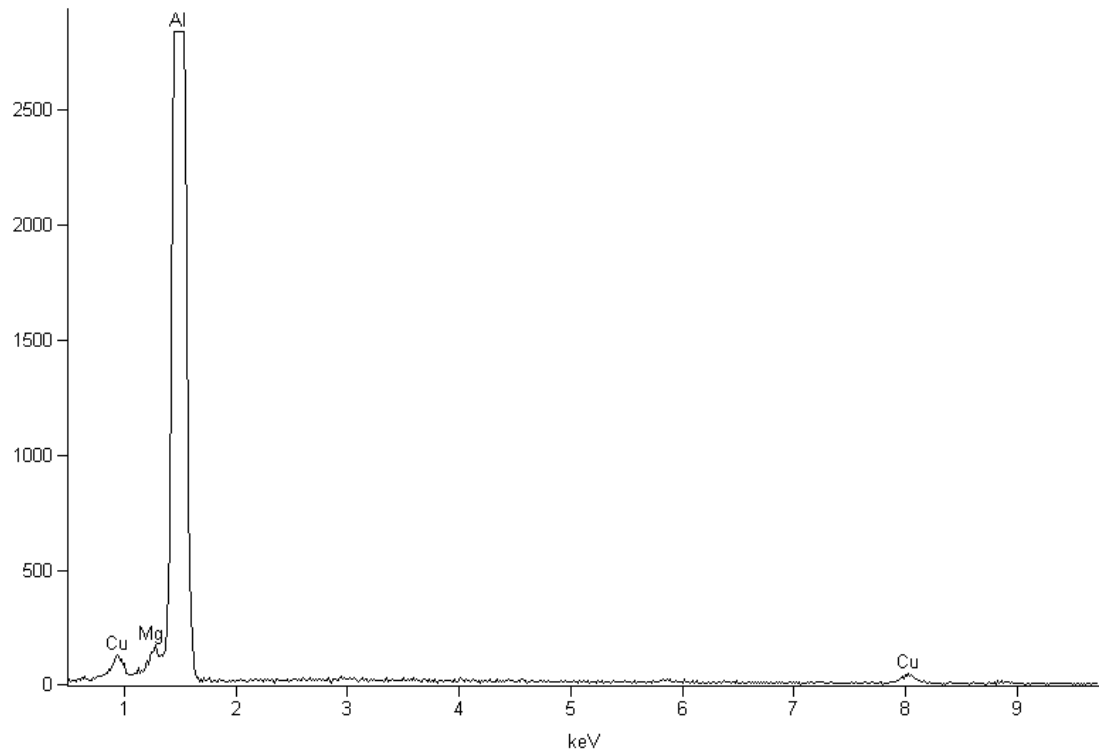


Figure A.2 EDS analysis of matrix in the solutionized specimen.

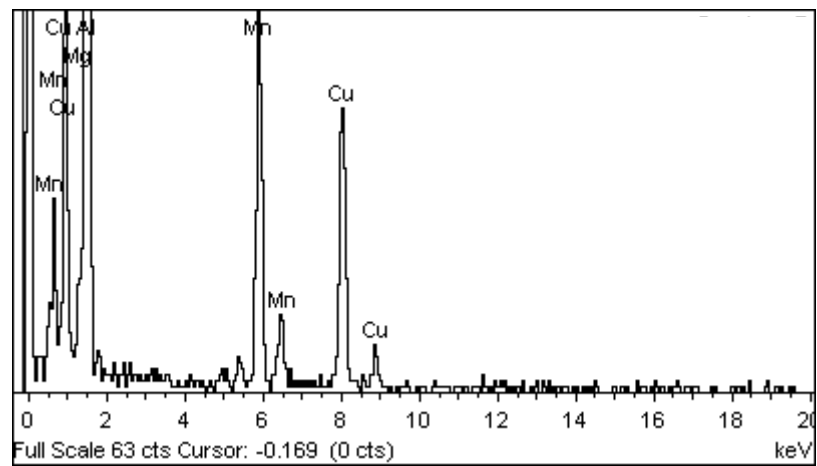


Figure A.3 EDS analysis of T-phase dispersoid in as-received specimen.

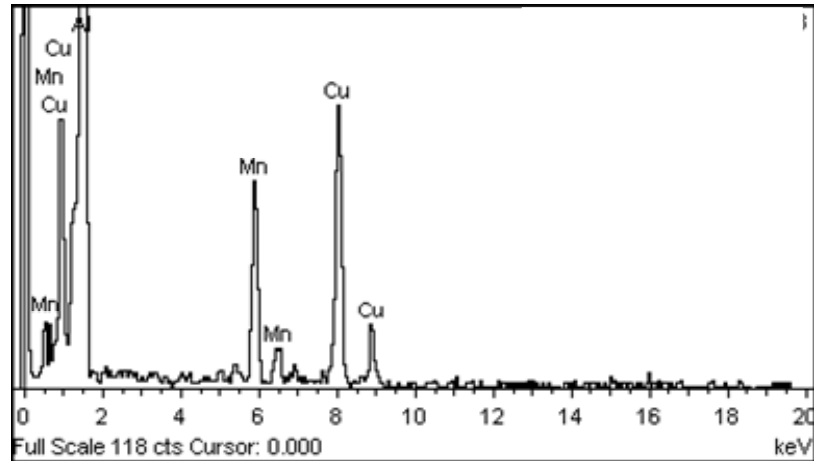


Figure A.4 EDS analysis of T-phase dispersoid in ECAPed specimen.

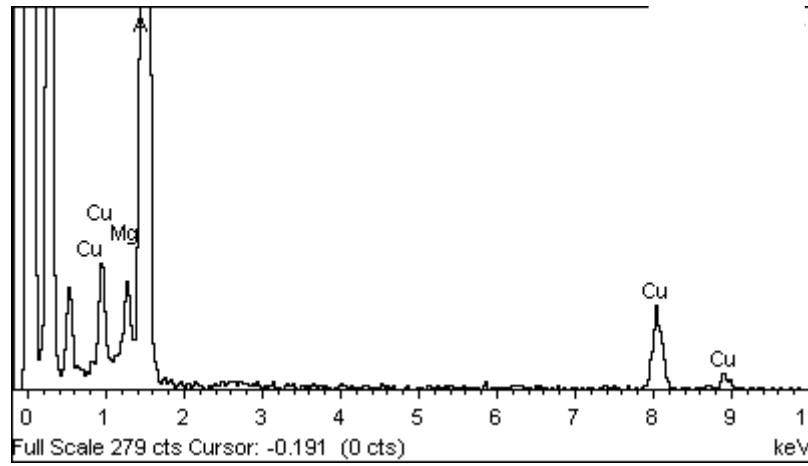


Figure A.5 EDS analysis of precipitates in the aged specimen.

APPENDIX B

X-RAY MAP ANALYSIS

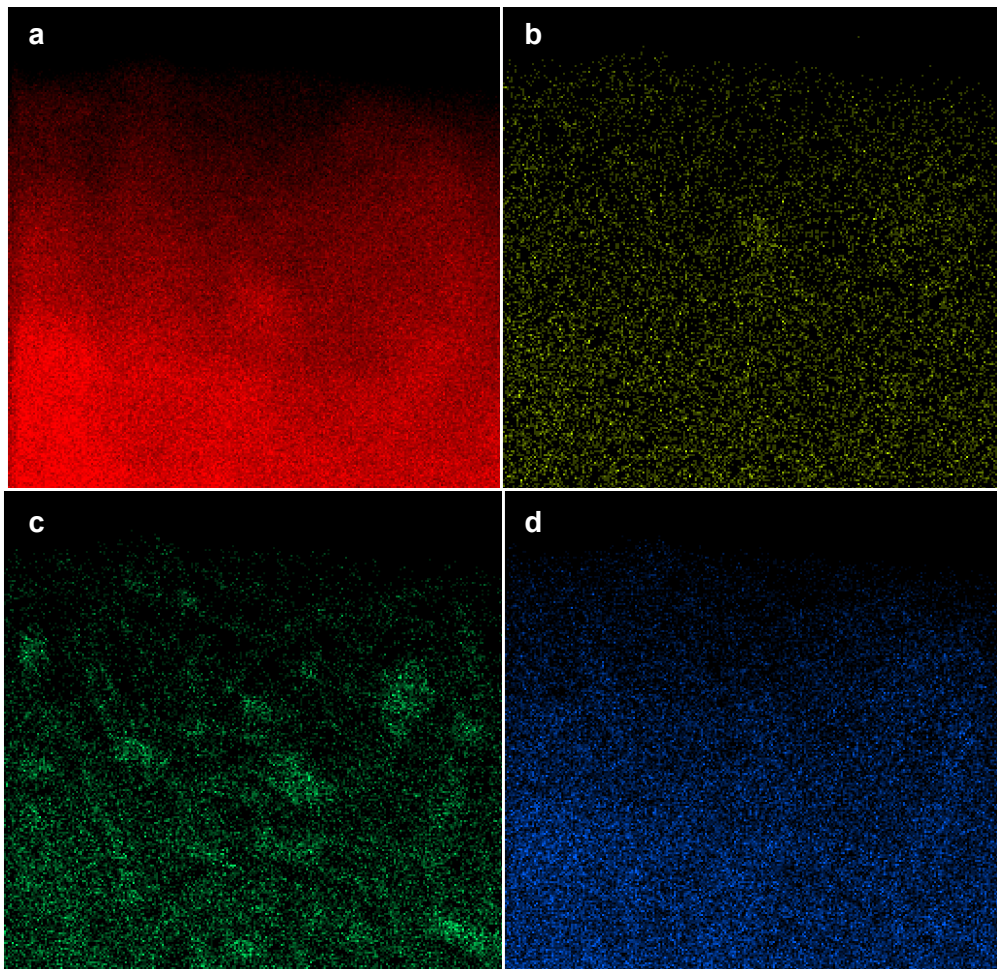


Figure B.1 X-ray map analysis of age hardened (190 °C / 12h) specimen showing **a.** Al, **b.** Si, **c.** Cu and **d.** Mg distribution.